# DESIGN OF COMPACT ANTENNAS IN MULTILAYER TECHNOLOGY FOR WIRELESS COMMUNICATIONS / WLAN APPLICATIONS

A Thesis Presented to the Academic Faculty

by

Gerald Reuben DeJean

In Partial Fulfillment of the Requirements for the Degree of
Masters of Science in Electrical and Computer Engineering

Georgia Institute of Technology

December 2, 2004

DESIGN OF COMPACT ANTENNAS IN MULTILAYER TECHNOLOGY FOR WIRELESS COMMUNICATIONS / WLAN APPLICATIONS

Approved by:

Dr. Emmanouil M. Tentzeris, Advisor
School of Electrical and Computer Engineering
*Georgia Institute of Technology*

Dr. Ioannis Papapolymerou
School of Electrical and Computer Engineering
*Georgia Institute of Technology*

Dr. Joy Laskar
School of Electrical and Computer Engineering
*Georgia Institute of Technology*

Date Approved: December 2004

ACKNOWLEDGEMENT

The author wishes to acknowledge the support of the Packaging Research Center and the Georgia Electronic Design Center. In addition, the author would like to thank Prof. Manos M. Tentzeris, Dr. Ronglin Li, Prof. John Papapolymerou, Prof. Joy Laskar, Dr. Stephane Pinel, Dr. Kyutae Lim, Dr. Nathan Bushyager, Edan Dalton, Jong Hoon Lee, Dane Thompson, and Eve Tsai for providing assistance in theoretical justification and insight, fabrication, and measurement setup used in this research. The motivation of living up to your dreams and reaching for the stars was instilled into the author's imagination by his parents Paula D. DeJean and Gerald R. DeJean, I, and maintained through the vision of Prof. Manos M. Tentzeris. For that, the author is eternally grateful. Lastly, the author would not have attained so much knowledge in the field of antenna design without the tireless efforts of Dr. Ronglin Li.

TABLE OF CONTENTS

LIST OF FIGURES

# LIST OF SYMBOLS AND ABBREVIATIONS

| | |
|---|---|
| 3D | Three Dimensional |
| AM | Amplitude Modulated |
| Co-pol | co-polarized |
| CP | Circular Polarization |
| CTE | Coefficient of Thermal Expansion |
| FCC | Federal Communications Commission |
| FDTD | Finite Difference Time Domain |
| FM | Frequency Modulated |
| GSM | Global System of Mobile Communications |
| GTRI | Georgia Tech Research Institute |
| IC | Integrated Circuit |
| ISM | Industrial-Scientific-Medical |
| LCP | Liquid Crystal Polymer |
| LMDS | Local Multipoint Distribution Systems |
| LTCC | Low Temperature Co-fired Ceramic |
| μBGA | Micro Ball Grid Array |
| MEMS | Micro-Electro-Mechanical Systems |
| MLO | Multilayer Organic |
| MMIC | Monolithic Microwave Integrated Circuit |
| PBG | Periodic Bandgap |
| RF | Radio Frequency |

| | |
|---|---|
| SAR | Specific Absorption Ratio |
| SHS | soft-and-hard surface |
| SMD | Surface Mount Device |
| SOP | System-on-Package |
| SPA | Shorted Patch Antenna |
| TE | Transverse Electric |
| TLM | Transmission Line Matrix |
| TM | Transverse Magnetic |
| UHF | Ultra High Frequency |
| VHF | Very High Frequency |
| VSWR | Voltage Standing Wave Ratio |
| WLAN | Wireless Local Area Networks |

## SUMMARY

The following document presents the design of two novel compact antennas architectures for wireless communications, wireless local area networks (WLAN) applications, automotive radar and millimeter-wave (mm-wave) applications. In recent years, the miniaturization of cell phones and computers has led to a requirement for antennas to be small and lightweight. Antennas, desired to operate in the WLAN or mm-wave frequency ranges, often possess physical sizes that are too large for integration with radio frequency (RF) devices. When integrating them into three-dimensional (3D) transceivers, the maintenance of a compact size also provides isolation from other devices, hence, surface wave propagation does not affect nearby components of the transceiver such as filters, baluns, and other embedded passives. Therefore, the development of a rigorous design method is necessary for realizing compact and efficient antennas in the wireless community. Furthermore, it is essential that these antennas maintain acceptable performance characteristics, such as impedance bandwidth, low cross-polarization, and high efficiency throughout a single or multiple frequency bands and standards.

In this work, various compact and packaging-adaptive antennas have been designed for practical wireless communications systems such as global system of mobile communications (GSM), Bluetooth Industrial-Scientific-Medical (ISM) devices, IEEE802.11a WLAN, and Local Multipoint Distribution Systems (LMDS) applications. First, compact stacked patch antennas using LTCC multilayer technology have been presented. A set of design rules is established for the purpose of designing optimized bandwidth compact antennas on LTCC multilayer substrates. To verify its effectiveness,

the proposed design rules are applied to three emerging wireless bands. The return loss and the impedance bandwidth are optimized for all three bands. A maximum bandwidth of 7% can be achieved for an antenna operating in the LMDS band.

Folded shorted patch antennas (SPAs) have been designed to significantly reduce the resonant frequency of a standard patch antenna. The design methodology of this structure starts with a conventional half-wave ($\sim\lambda_0/2$) and through a series of procedures, evolves into a smaller, $\sim\lambda_0/8$ resonant length structure. Upon varying the height of the lower patch, the resonant length can be reduced to $\sim\lambda_0/16$. A comparison between a folded SPA and a standard SPA validates the folding technique proposed in this document. The folded SPA is applied to the 2.4 GHz ISM band. The measured results are in good agreement with simulated results. This antenna can be implemented into 3D packages using multilayer laminates such as LTCC or LCP.

# CHAPTER 1

# INTRODUCTION

Due to the emergence of the communications industry, which has taken place over the last 60 years, antennas and their principles have been an important area of focus. Antennas can be incorporated in various geometries and can be used in several applications. Dipole antennas, or "dipoles", (Figure 1a) and monopole antennas, or "monopoles", are common straight wire antennas that exhibit omni-directional radiation. The main difference between dipoles and monopoles is their physical configuration. Dipoles have two separate conducting wires, one connected to the positive terminal and the other connected to its negative counterpart. By using image theory, the monopole can be realized by removing one conducting wire and replacing it with a ground plane, hence reducing the size by one half. These antennas can be used to improve reception of frequency modulated (FM) broadcast signals. They are still active in the cellular phone industry as well. Loop antennas (Figure 1b), which were utilized as far back as the late 1910s, offer very directional radiation. These antennas are a variation of dipoles and can be constructed by simply shaping a straight wire into a loop taking many forms, such as rectangular, triangular, and circular, and being primarily used for amplitude modulated (AM) broadcast and longwave bands. The pyramidal horn (Figure 2a), the conical horn (Figure 2b), and the rectangular waveguide (Figure 2c) are all examples of aperture antennas that radiate energy through aperture cross-sections. Horn antennas typically possess a large gain and are used as feeding elements for reflector antennas. These are also useful for aircraft and spacecraft applications because they can be flush mounted on the skin of the aircraft or spacecraft [1].

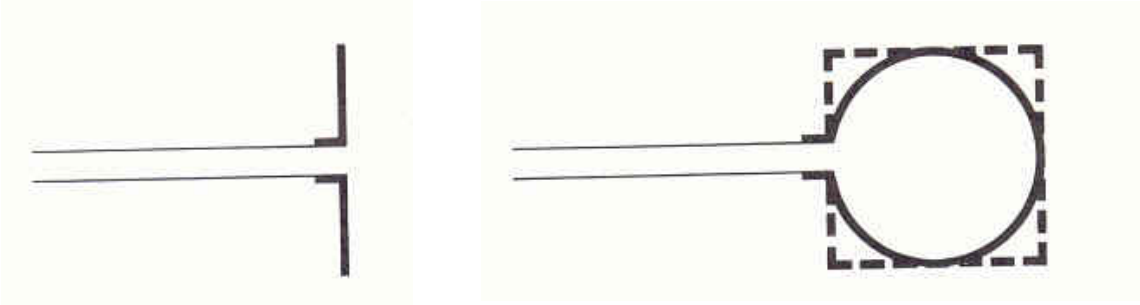

a. b.

Figure 1. (a) dipole antenna, (b) loop antenna [1].

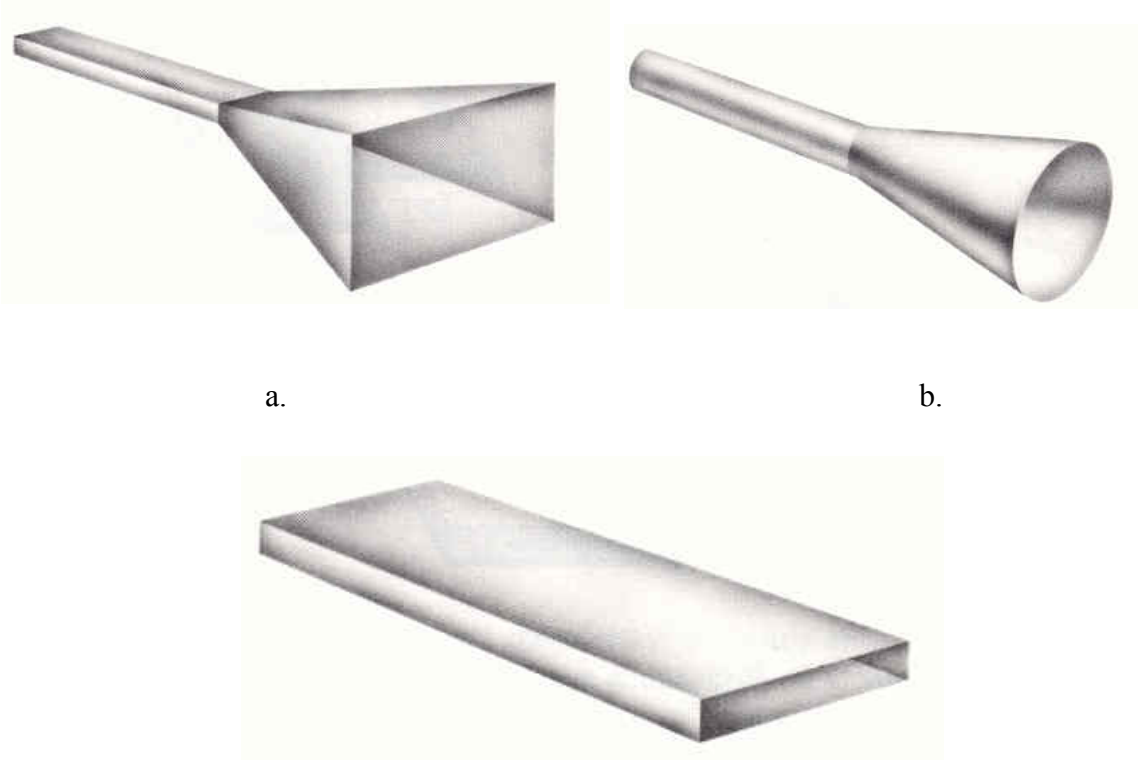

a. b.

c.

Figure 2. (a) pyramidal horn, (b) circular horn, (c) rectangular waveguide [1].

Finally, reflector antennas, such as the parabolic reflector and the corner reflector, allow the transmission and reception of signals over long distances. These antennas operate by utilizing a feeding horn antenna that transmits radio waves that reflect off of a large conducting plane in the opposite direction (Figures 3a and 3b). This is analogous to the reflection of someone's image as he looks in the mirror. In today's consumer market, DirecTV is a common service that provides digital television entertainment and broadband satellite networks to thousands of homes around the world. This is done through the use of reflector antennas (Figure 4).

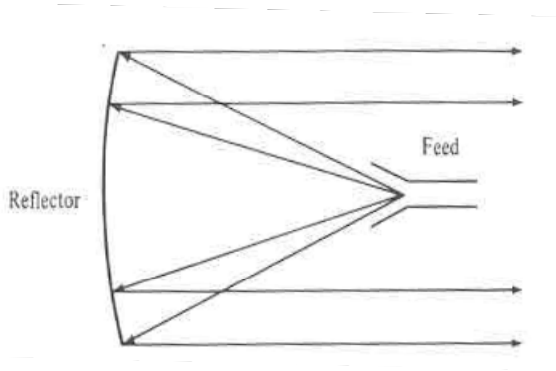


a.

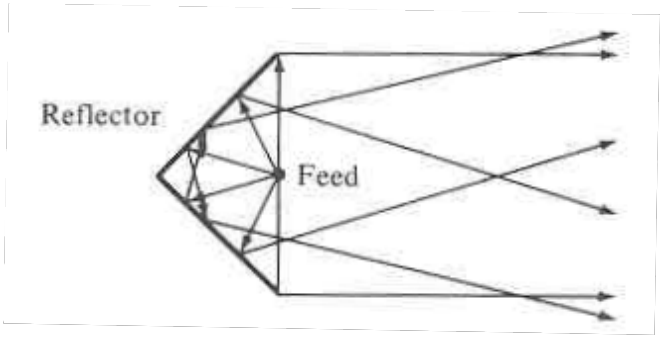


b.

Figure 3. (a) parabolic reflector antenna, (b) corner reflector antenna [1].


Figure 4. DirecTV satellite dish

Each of the aforementioned antennas has a large physical size that is not suitable for compact wireless communications transceivers and RF modules. To overcome this limitation, microstrip (Figure 5) or planar antennas [2,3,4], that are printed on a dielectric substrate backed by a conducting ground plane, present an effective solution to the development of miniaturized structures. Since the antennas are resonant structures, the need for additional passive circuitry to assist in achieving resonance is alleviated. Microstrip antennas have received much consideration for implementation in system-on-package (SOP) technology. SOP technology consists of a multifunction, multichip package that enables the integration of many system-level functions, such as digital, optical, analog, and micro-electro-mechanical systems (MEMS) [5,6]. Additionally, SOP enables three-dimensional (3D) compact architectures to be realized. Planar antennas can be integrated into 3D modules for millimeter-wave short range broadbands and reconfigurable sensor networks.

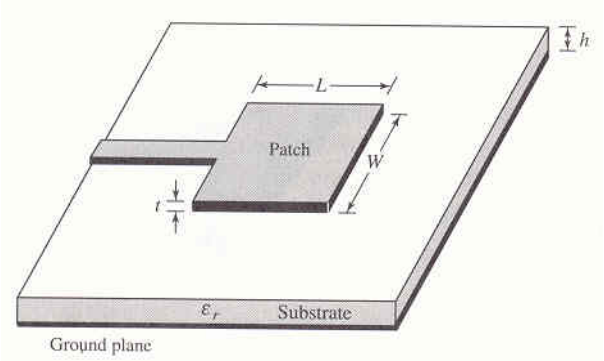


Figure 5. microstrip antenna [1].

These structures enjoy many advantages over their counterparts, such as low manufacturing cost via modern printed circuit technology, low profile, ease of integration with monolithic microwave integrated circuits (MMICs) and integrated passives, and the ability to be mounted on planar, nonplanar, and rigid exteriors [7]. Low temperature co-fired ceramics (LTCC) multilayer technology is becoming more and more popular for producing complex multilayer modules and antennas due to its flexibility in realizing a variable number of laminated layers [8,9]. Major advantages of using LTCC are lower dielectric loss, size reduction due to high dielectric constant, hermeticity, ability to integrate surface mount devices (SMDs) and integrated circuits (ICs), and ability to incorporate embedded passives and interconnect circuitry to be sandwiched between the substrate layers. The high dielectric constant of LTCC is significant in realizing more compact 3D architectures due to the inversely proportional relationship between the dimensions and the dielectric constant. Designing microstrip antennas on LTCC layers offers a desirable approach for integration with RF devices. To increase the physical area of the antenna, one can place air vias in the structure which will, in turn, lower the effective dielectric constant and produce a larger physical area. Some disadvantages

associated with LTCC are the shrinkage of the material and the surface wave excitation due to the high dielectric constant of the substrate. Alternative organic materials, such as the liquid crystal polymer (LCP), offer certain advantages over LTCC. These include a lower cost, engineered transverse coefficient of thermal expansion (CTE), and flexibility, although this is a less mature fabrication technology [10].

When designing planar antennas for wireless communications, it becomes necessary to have a microstrip antenna that is compact in size and able to be integrated with other devices. With the physical area of the antenna being inversely proportional to the frequency, it is sometimes difficult to achieve a compact size for WLAN applications for acceptable efficiency and isolation values. Furthermore, reducing the height of the structure may appear to be a suitable solution, but it may lead to a reduced impedance bandwidth and lower radiation efficiency. There is often a tradeoff in realizing compact antennas while maintaining performance characteristics.

This document discusses the design strategy and analysis of two compact antenna structures for wireless communications and WLAN applications. This is a general approach with the goal of operational use for many frequency bands and standards with acceptable performance characteristics. The LTCC multilayer technology is utilized when necessary for integration with 3D modules. These antenna designs are not limited to only LTCC structures, but can be extended to all multilayer laminated organic and ceramic substrates. Simulated and measured results are presented to support the design methodology implemented for the realization of compact antennas.

# CHAPTER 2

# BACKGROUND

Compact microstrip antenna design has been a "hot" topic of discussion in order to meet the miniaturization requirements of portable communication equipment [11]. Many attempts have been made to decrease the size of antennas from reducing the substrate thickness to using a substrate with a high permittivity. An overview of previous design methods for compactness and operational maintainability will be presented. This will be done in three parts. The first part will focus on what has been done to realize compact microstrip antennas. Next, past techniques will be described to show how compact antennas can be applied to achieve specific performance characteristics, such as enhanced bandwidth and gain, dual frequency operation, and circularly polarized radiation. The final part will detail some complexities associated with designing compact antennas for integrated transceivers and wireless applications.

## 2.1 HISTORY OF COMPACT DESIGN

Various techniques have been documented to reduce the size of microstrip antennas for a given frequency. The simplest method is to use a high dielectric constant substrate [1,2,11]. This can be justified by understanding that microstrip antennas are approximately half-wavelength structures, meaning that the resonant length is half of a guided wavelength ($\lambda_g/2$). One guided wavelength can be expressed as the ratio of the phase velocity ($v_p$) to the frequency (f). Additionally, the phase velocity can be expressed as the ratio of the speed of light ($c \approx 3*10^8$) to the square root of the effective dielectric constant. In equation form, the length of a microstrip antenna is approximately

$$L = \frac{c}{2f\sqrt{\varepsilon_{eff}}} \tag{1}$$

The effective dielectric constant increases with increasing dielectric constant [4]. Depending on the process and application, the dielectric constant may remain a fixed parameter; a high dielectric constant will maintain the compactness of the structure, while a low dielectric constant will result in a more efficient radiator. If this dielectric constant has a high value, surface modes may be launched at the interface of the air and dielectric material. Surface waves are transverse magnetic (TM) and transverse electric (TE) modes which propagate into the substrate outside the microstrip patch [12]. These modes have a cutoff frequency which is different than the resonant frequency for the dominant mode of the antenna. Surface waves become a problem when their cutoff frequency is lower than the resonant frequency of the antenna causing overmoding (more than one propagating mode at a given frequency). The cutoff frequency of a surface wave is inversely proportional to the dielectric constant of the substrate. This is shown in the formula below:

$$f_c = \frac{nc}{4h\sqrt{\varepsilon_r - 1}} \tag{2}$$

where c is the speed of light ($c \approx 3*10^8$), h is the substrate thickness, $\varepsilon_r$ is the dielectric constant, and n=1,3,5…for $TE_n$ modes and n=2,4,6…for $TM_n$ modes. If surface waves are present, the total efficiency of the antenna will be reduced. There is often a tradeoff between compact size and efficiency. Therefore, other methods have been proposed to

reduce antenna dimensions with fixed substrate properties. One method is the use of a meandered patch (Figure 6). The meandering is done by cutting slots in the non-radiating edges of the patch [13,14]. This effectively elongates the surface current path on the patch and increases the loading which results in a decrease in the resonant frequency.

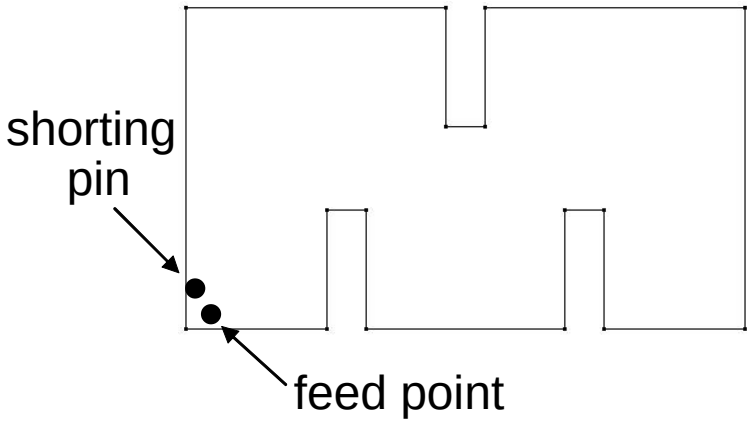


Figure 6. Meandered patch by inserting slots in non-radiating edges [14].

The tradeoff that is seen in using this method is a decrease in impedance bandwidth and antenna gain, that causes a severe limitation in practical applications [15]. Additionally, high levels of cross-polarization may arise from sections of the meandered patch [16].

Another method includes the meandering of the ground plane [15]. In a similar approach, the insertion of slots in the ground plane can reduce the resonant frequency for a given length (Figure 7).

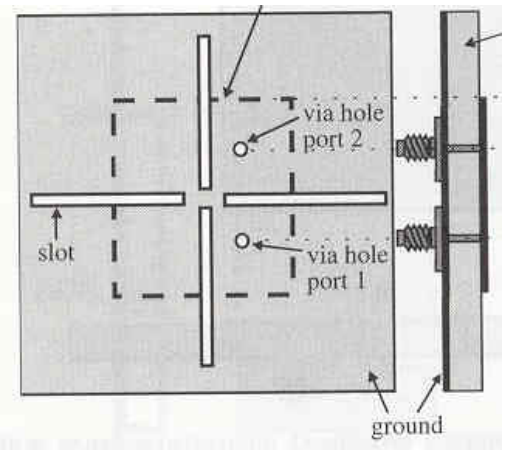


Figure 7. Meandered patch by inserting slots in ground plane [15].

The slots of the ground plane may cause unwanted levels of backside radiation [17], leading potentially to high absorption of energy from the human head when the antenna is used in PCS applications, specifically when the antenna is placed in cellular phones [18]. This absorption of radiation to the head is characterized by the specific absorption ratio (SAR). An acceptable SAR level required by the Federal Communications Commission (FCC) for public exposure is 1.6 W/kg [19]. Another popular technique involves a shorted plane that is placed along the middle of the patch parallel to the radiating edge between the patch and the ground plane. With the presence of the shorted plane, half of the patch can be omitted. The patch now has a resonant length of a quarter-wavelength ($\lambda/4$). Theoretically, the position of the shorted plane is selected where the electric field normal to the patch is non-existent. Therefore, the fields parallel to the shorted plane are undisturbed. The major disadvantage of this method is a narrower impedance bandwidth for some applications, such as DECT (digital European cordless telephones) [20]. Also, punching vias through the substrate to create the shorted patch may not be suitable for

some materials, such as LCP, due to the alignment inaccuracies of the vias. Targonski and Waterhouse attempted to alleviate this problem by using a thick foam substrate with a low dielectric constant [35], but this affected the compactness of the antenna. The low-cost use of foam may not be suitable for RF packaging applications that involve a high temperature environment. Finally, the use of varactor diodes (Figure 8) has been shown to contribute to compact operation by means of tuning the resonant frequency [21]. Varactor diodes contain a capacitance which can be adjusted by changing their voltage. This additional capacitance helps to decrease the resonant frequency making for a more compact geometry. This structure could also support circularly polarized radiation.

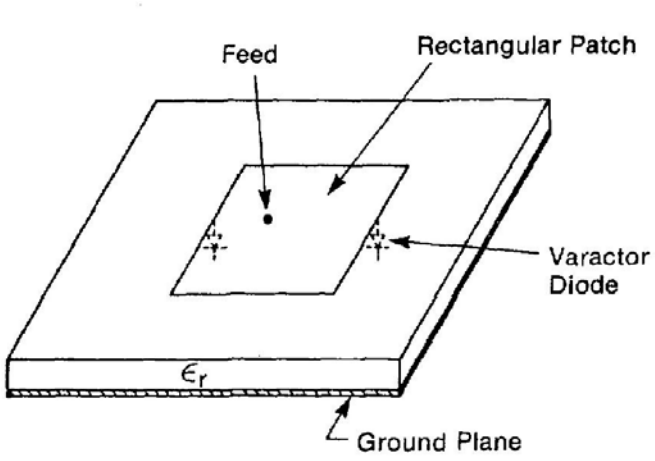


Figure 8. Patch antenna loaded with varactor diodes [21].

One concern from this approach is that the close distance between a varactor diode and the coaxial probe can cause unwanted coupling, while widening this distance by moving the probe may destroy the impedance match. Additionally, although a large bandwidth can be achieved, reduced efficiency and increased levels of cross-polarization are present [22]. Ultimately, the use of varactor diodes presents a problem in terms of integrating the

antenna into an RF module. Many times, devices operating in the very high frequency (VHF) and the ultra high frequency (UHF) require antennas to be completely passive elements. Therefore, a varactor diode (an active component) would have to be realized in terms of a printed component instead. Du Plessis and Cloete proposed a solution of using a metallic pad at the radiating edges of a rectangular patch [23]. This design, shown in Figure 9, is completely passive and has the similar feature of changing the resonant frequency of the antenna. When the size of the pads is determined and the antenna is fabricated, a trimming device could be used to trim off metal from the pads.

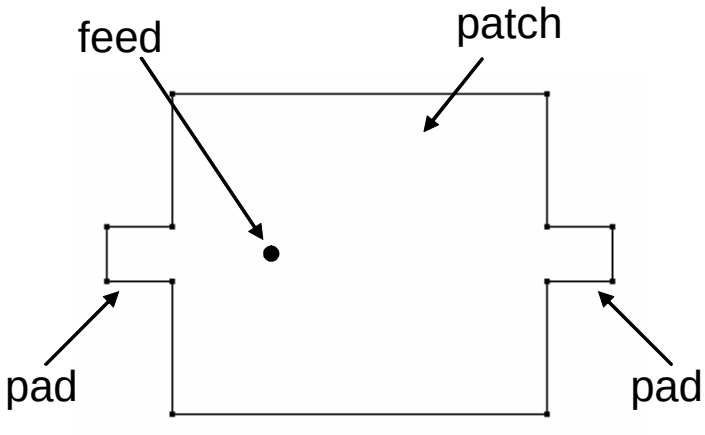


Figure 9. Patch antenna loaded with metallic pads.

By doing this, the antenna's resonant length is shorter due to the shorter surface current path; hence, the resonant frequency can be increased. With this method, the frequency of operation cannot be decreased. Also, the trimming of the antenna may affect the performance of the design. The idea of modifying a structure once it has been fabricated is often not practiced in RF packaging and antenna design.

## 2.2 PREVIOUS TECHNIQUES IN PERFORMANCE ENHANCEMENT

Compact antenna design can be utilized to achieve circular polarization (CP), enhanced gain, and wideband operation for many applications, such as GPS, Bluetooth and WLAN applications. Recent attempts have been made to realize these performance characteristics. One of the simplest ways to attain circular polarization is to insert a cross-shaped slot in the patch [36,37]. This tends to excite two orthogonal modes with a 90° phase difference between them, a necessary condition for CP. This method is useful because it only requires a single feed point. Trimming off the corners of the patch along the same diagonal direction (Figure 10) is another means of achieving CP while maintaining a compact design [24].

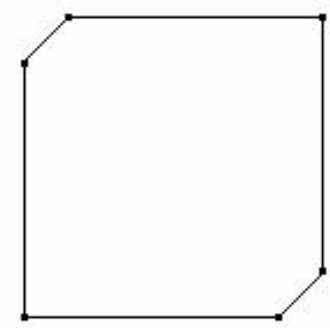

Figure 10. Patch antenna with trimmed corners.

An additional simple approach can be taken where one can slightly increase the length (or width but not both) of a square patch. This makes the patch "nearly square". Using this technique as well as exciting the patch along the diagonal, achieves CP by obtaining two modes with slightly different resonant frequencies. One mode can "lead" by 45°, while the other mode can "lag" by 45°; hence, a 90° phase difference is produced while maintaining electric field amplitudes that are equal [25,26]. An advantage to this design

is the ease in which CP can be achieved. The circuit modeling and radiation characteristics for this approach remain unchanged. Despite the advantages, there has been no formulated approach of choosing the correct length perturbation to achieve CP. There are few designs that have been reported for producing enhanced gain while maintaining compact operation. One of these designs incorporates two substrate layers with the patch antenna embedded between them (Figure 11). The lower substrate (between the patch and the ground plane) has a low dielectric constant ($\varepsilon_r < 5$), while the other substrate layer (above the patch) has a high dielectric constant ($\varepsilon_r > 15$) [27,28]. This high dielectric constant will excite substrate modes, thus lowering the efficiency and bandwidth which may not be suitable for a desired application [17].

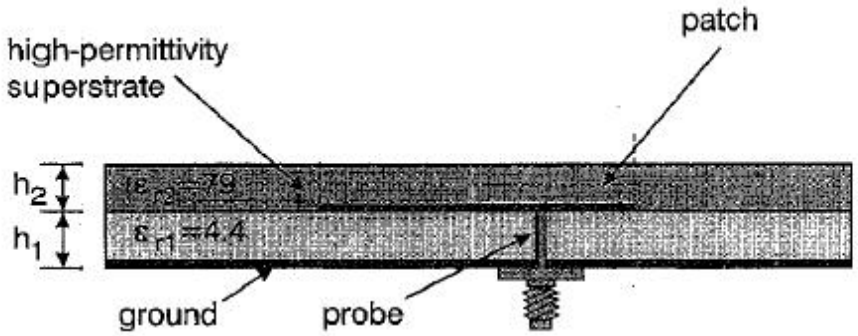


Figure 11. Patch antenna with low and high permittivity substrate [28].

Another technique that can be used for enhancing the gain of microstrip antennas involves placing parasitic elements next to the radiating patch [38]. The radiating patch will capacitively couple energy to the nearby parasitic elements creating a wider aperture. Although this wider aperture will increase the gain of the structure, the effect may not be significant. A possible drawback using this approach is the increased lateral area of the design which may prohibit the compactness of the structure. Careful placement of the

parasitic elements must also be taken into account. Placing these elements too close to the radiating patch can greatly decrease the resonant frequency of the antenna, while positioning the elements too far from the radiating patch will exhibit no effects at all. Finally, the achievement of wideband frequency operation has been reported in [11]. In addition to stacking, one design incorporates an aperture-coupled shorted patch with a slot in the ground plane. The uniqueness of this design is the thick air substrate employed under the patch [29]. With the length and width of the patch chosen to resonate at two frequencies that are close to each other, the use of the air substrate helps to widen the bandwidth to a point where it combines to cover the bandwidth of both resonant frequencies. With this design, a total impedance bandwidth of 26% can be achieved. A second compact design with wideband operation utilizes a chip resistor that is placed between the patch and the ground plane at one radiating edge of the structure [30]. The wideband effect can be seen by considering the decrease in the quality factor, or Q-factor, when additional resistance is introduced into the circuit. This decreased Q-factor greatly increases the bandwidth of the antenna as observed in the equation below:

$$BW = \frac{S-1}{Q\sqrt{S}} \tag{3}$$

where BW is the bandwidth and S represents the maximum voltage standing wave ratio (VSWR) value that is desired for an acceptable impedance match. For antennas, this value is usually equal to 2. The major disadvantage of this design is the reduced efficiency since a large portion of the input power is dissipated in the resistor which takes away available power that can be radiated by the antenna.

## 2.3 DESIGN COMPLEXITIES

Despite the fact that much work has been done in the area of compact antenna design, there exist some design complexities that must be taken into account. One complexity arises from the use of a high dielectric constant substrate. High dielectric constant substrates are favored for miniaturization of structures, but surface modes are launched into the substrate, which reduces the radiated power, thus significantly reducing the efficiency of the antenna [17]. Another complexity stems from the feeding structure. Some designers prefer to use microstrip lines printed on the same layer as the antenna for excitation. Ease of fabrication and simplicity in circuit modeling are two of the advantages of using these lines. Unfortunately, radiation loss of microstrip lines increase as the ratio of the square of the length to the square of the free space wavelength ($L^2/\lambda^2$) increases [31]. The radiation from the microstrip line may also tilt the main beam a few degrees in the direction of the feed line [32]. A coaxial cable may be suitable for excitation, but depending on the substrate, this may not be possible to manufacture. Additional feeding methods have been utilized when a planar design is necessary. In particular, proximity-coupling and aperture-coupling are two of the more popular feeding methods due to the decreased levels of cross-polarization and the shielding of the feedline radiation by the ground plane (applicable only in aperture-coupling) [39]. The proximity-coupled feeding is capacitive in nature while the aperture coupled feeding is inductive. The lack of design rules can cause the analysis of both feeding techniques to be complex. Moreover, these feeding methods can only be utilized in a multilayer environment, but they can take full advantage of the 3D integration. This places an additional restriction on the design which may not be suitable for the desired application. It is important to

maintain the effectiveness of the antenna by taking into account all complexities that are associated with a design.

# CHAPTER 3

# COMPACT STACKED PATCH ANTENNAS USING LTCC MULTILAYER TECHNOLOGY

The stacked patch antenna is a common approach for achieving a wider impedance bandwidth. One problem with using a stacked structure is the distance between the two antennas may possibly shift the design frequency. In addition, there are many parameters that need to be adjusted for an optimal bandwidth performance, such as the length and width of each patch, the thickness of the substrate, as well as the position of the feed point. With so many parameters that need to be accounted for, to date, there has been no control over adjusting all variables, simultaneously, to achieve optimal bandwidth performance. Therefore, there is a need for a set of design rules to guide antenna engineers in designing wideband antennas.

## 3.1 ANTENNA STRUCTURE

The integration concept of 3D modules that is considered in this chapter is illustrated in Figure 12. A stacked-patch antenna is embedded on the top of an RF frond-end module in an LTCC multilayer package. The input of the antenna comes from the output of an embedded band-pass filter that is connected with a block of RF active devices by processes called “flip-chipping” and “wire-bonding”. The vertical integration capabilities in the LTCC technology provide the space for the embedded RF block. The LTCC cavity process also provides integration opportunities for RF passive components such as switches or/and off-chip matching networks. The vertical board-to-board transition of two LTCC substrates is implemented using a micro ball grid array (μBGA) ball process.

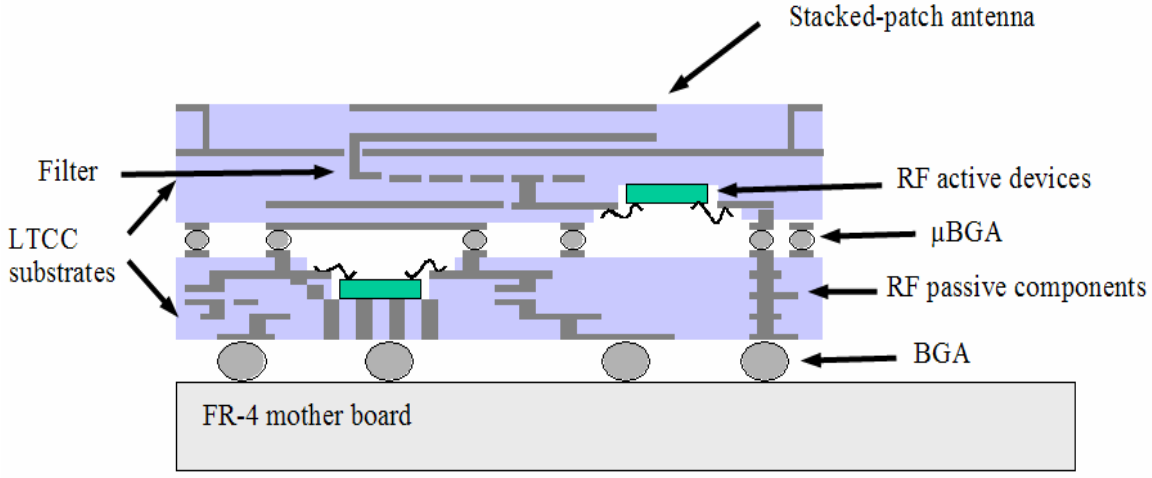


Figure 12. 3D integrated module.

The standard BGA balls insure the interconnection of the highly integrated LTCC module with a mother board such as a FR-4 substrate.

The antenna structure for this design is shown in Figure 13. It consists of two square patches (lower and upper) of length L that are stacked on a grounded LTCC substrate. Square patches were used in this design for the purpose of two orthogonal modes, $TM_{10}$ and $TM_{01}$, with resonant frequencies that are in close proximity to each other, therefore, obtaining a wider bandwidth. The total thickness of the substrate is denoted h. This thickness can be divided into two smaller thicknesses, $h_1$, the distance between the lower patch and the ground plane, and $h_2$, the distance between the lower and upper patch where $h=h_1+h_2$. The lower patch of the antenna structure is excited through a via that is connected to the output port of a filter. A via is a slender piece of metal that vertically connects components on different layers. Then, electromagnetic coupling of energy is transferred from the lower patch to the upper patch. The position of the (via) is placed at the center of the radiating edge in order to match a 50 ohm coaxial line.

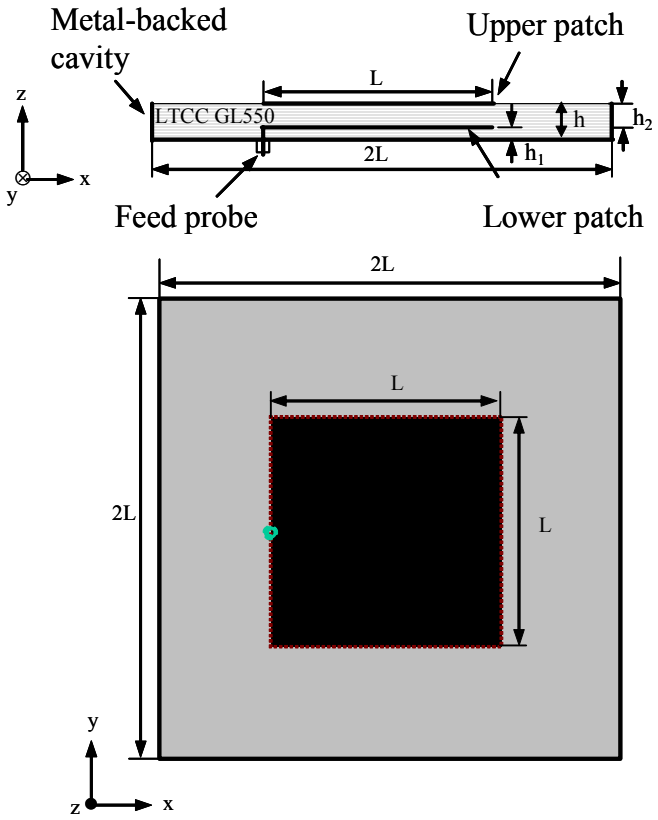


Figure 13. Stacked-patch antenna architecture on LTCC multilayer substrate.

In the 3D RF front-end module, the antenna is integrated with other RF circuits. It is essential to prevent any unwanted radiation from other RF components in the integrated module. Therefore, a metal-backed cavity is introduced in order to shield the RF signals of components surrounding the antenna from the separate antenna signals to preserve functionality. In LTCC packaging technology, a continuous metal wall cannot be realized in fabrication. This obstacle is overcome through the use of an array of vertical vias. It is recommended to choose the lateral dimension of the cavity to be twice that of the stacked patch. A smaller dimension may result in reflections from the walls,

which may affect the impedance characteristics of the antenna and hence, the bandwidth of the structure. A larger dimension may hinder the compactness of the structure.

## 3.2 THEORETICAL ANALYSIS

Besides the use of square patches in increasing the bandwidth, the major contribution in the wide-bandwidth performance of the stacked-patch antenna is achieved through the combination of two close resonant frequencies which respond respectively to the lower patch and the upper patch. The combination is made by an electromagnetic coupling between the two patch resonators, which can be modeled by the equivalent circuit shown in Figure 14.

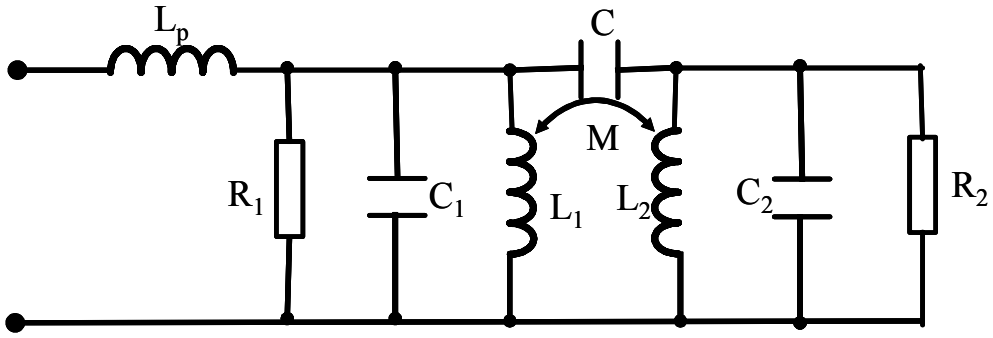


Figure 14. Equivalent circuit of the probe-fed stacked-patch antenna.

This circuit consists of two electromagnetically coupled parallel resonant circuits where $L_1$ and $L_2$ are equivalent inductances, $C_1$ and $C_2$ are equivalent capacitances, and $R_1$ and $R_2$ are radiation resistances. (Subscript 1 refers to the lower patch and subscript 2 refers to the upper patch.) A series inductance, $L_p$, is included to model the inductance of the feed probe [4]. Two resonant frequencies depend on $L_1C_1$ and $L_2C_2$. This is shown in the formula below:

$$f_n = \frac{1}{2\pi(L_n C_n)} \tag{4}$$

where n = 1,2. Furthermore, the tightness of the electromagnetic coupling is decided by the coupling capacitance C and mutual inductance M. By adjusting the heights of the lower and upper patches, the corresponding resonant frequencies and the coupling tightness can be varied, thus resulting in an optimal impedance performance.

## 3.3 PRELIMINARY STUDY

Simulations of this structure using Microstripes 5.5 were performed, and initial results were taken and analyzed. Microstripes 5.5 is a 3D fullwave simulator by Flomerics Ltd. which uses transmission line matrix (TLM) modeling for analysis. First, a comparison was done to show the variation of input impedance as a function of frequency for five values of relative dielectric constant: $\varepsilon_r$ = 2, 4, 6, 8, and 10. This is shown in the form of a Smith chart (Figure 15). A circle labeled "vswr 2:1" represents a reflection coefficient of one-third and a -10 dB return loss. The plot of the input impedance inside this circle shows the -10 dB return loss bandwidth that can be achieved for the particular frequency band. The more input impedance points that lie in the "vswr 2:1" circle, the wider the bandwidth of operation. The horizontal center line of the Smith chart represents a purely resistive impedance. An impedance above this line is resistive and inductive, while an impedance below this line is resistive and capacitive. The impedance loop tends to move downward as the dielectric constant increases. This is a result of the increased parallel plate capacitance due to the proportional relationship between the

capacitance and the dielectric constant. Additionally, the parallel plate capacitance is inversely proportional to the plate separation.

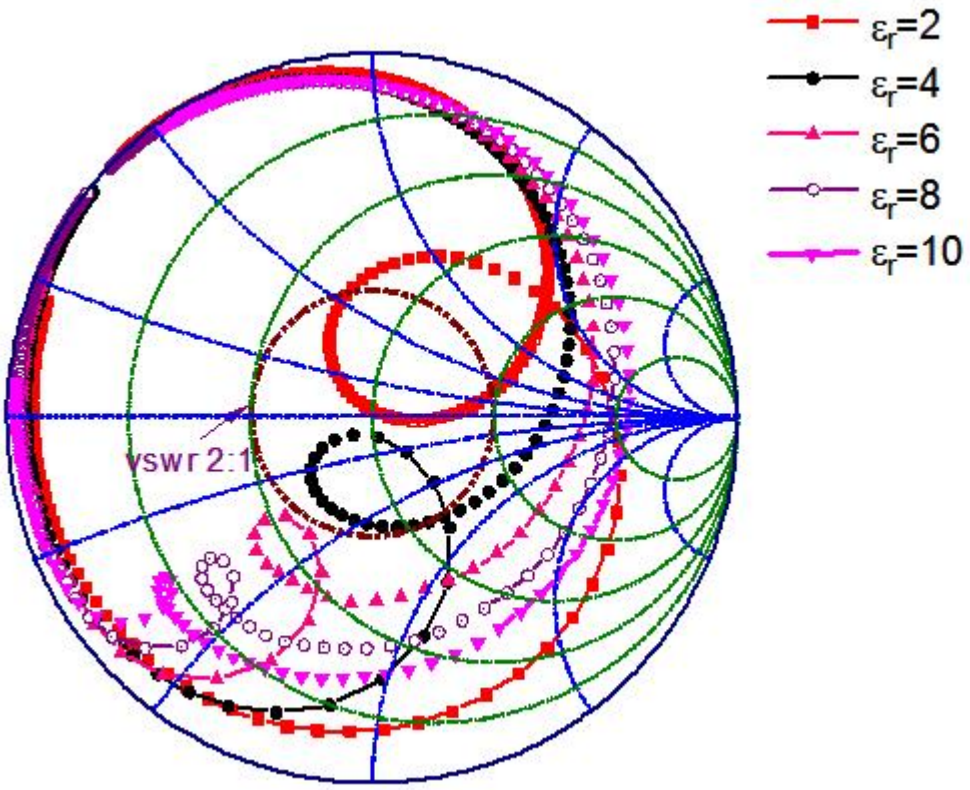


Figure 15. Smith chart of input impedance for variable values of $\varepsilon_r$.

The formula for the capacitance C of two finite size plates with a finite separation distance from each other is shown below:

$$C = \frac{\varepsilon_r \varepsilon_o A}{d} \tag{5}$$

where $\varepsilon_r$ is the dielectric constant, $\varepsilon_o$ is the permittivity of free space, A is the lateral area of the plate, and d is the separation distance of the plates. For this simulation, the length

and width of both patches is each 10 mm. The distance from the parasitic patch to the excited patch is 1 mm. The distance from the excited patch to the ground is also 1 mm.

A second simulation was done to analyze the effect of changing the position of the excited patch. By doing this, the input impedance bandwidth can be optimized. Figure 16 shows the input impedance as a function of frequency for a fixed dielectric constant ($\varepsilon_r$ = 7) in the form of a Smith chart. It can be observed that a position of 0.5 mm above the ground plane gives an impedance loop that is totally inside the "vswr 2:1" circle, hence, an optimal bandwidth. It is also clearly shown that the impedance loop moves downward as the height of the excited patch (distance from the ground plane) increases. This simulation was done for a stacked patch structure where each patch has a length and width of 10 mm. The total substrate thickness is 2 mm.

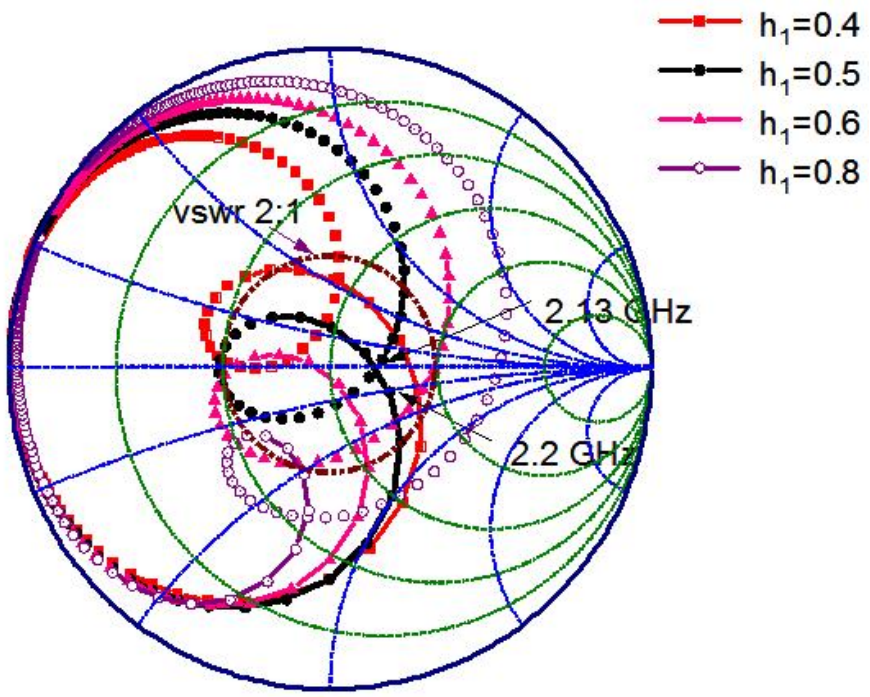


Figure 16. Smith chart of input impedance versus frequency for variable values of lower patch height at $\varepsilon_r$ = 7.

Another simulation was done to also analyze the effect of changing the positioning of the excited patch. Figure 17 shows the input impedance as a function of frequency for a fixed dielectric constant ($\varepsilon_r = 5$) in the form of a Smith chart. It can be observed that a position of 0.6 mm above the ground plane gives an impedance loop that is totally inside the "vswr 2:1" circle, and therefore, a bandwidth that is optimal. It is again clearly shown that the impedance loop moves downward as the height of the excited patch above the ground plane increases. This simulation was done for a stacked patch structure where each patch has a length and width of 10 mm. The total substrate thickness is 2 mm.

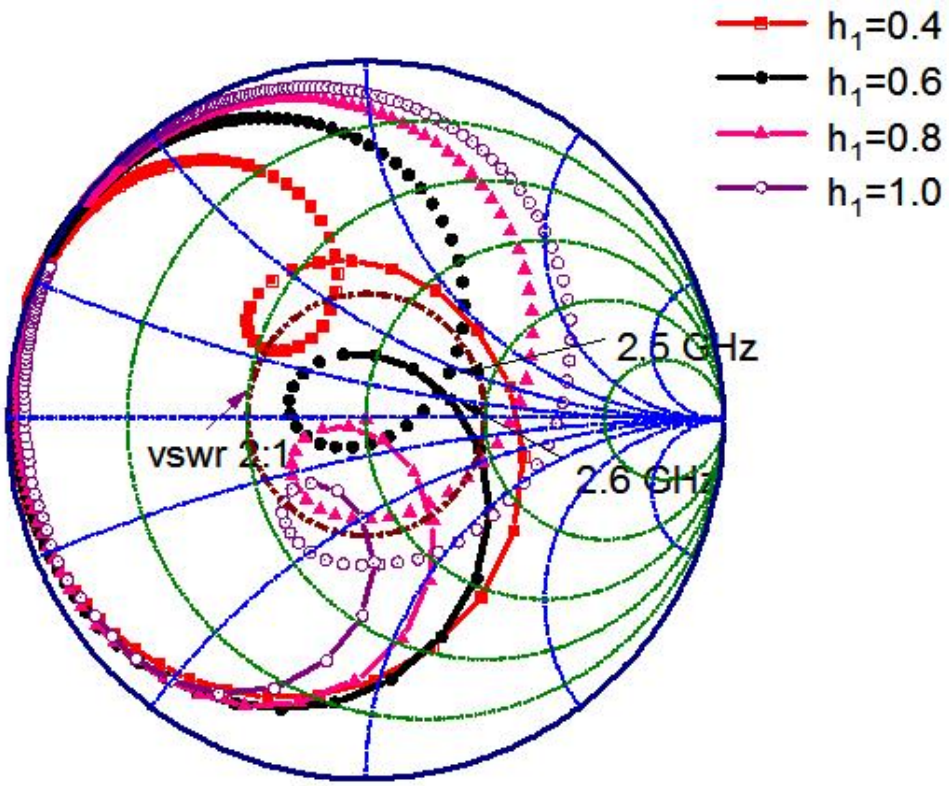


Figure 17. Smith chart of input impedance versus frequency for variable values of lower patch height at $\varepsilon_r = 5$.

A final simulation was done to examinee the effect of changing the positioning of the excited patch. Figure 18 shows the input impedance as a function of frequency for a fixed dielectric constant ($\varepsilon_r = 3$) in the form of a Smith chart. The Smith chart shows that a position of 1 mm above the ground plane will give an impedance loop that is totally inside the "vswr 2:1" circle, and therefore, an optimal bandwidth. It is again clearly shown that the impedance loop moves downward as the height of the excited patch increases. This simulation was done for a stacked patch structure where each patch has a length and width of 10 mm, and the total substrate thickness is 2 mm.

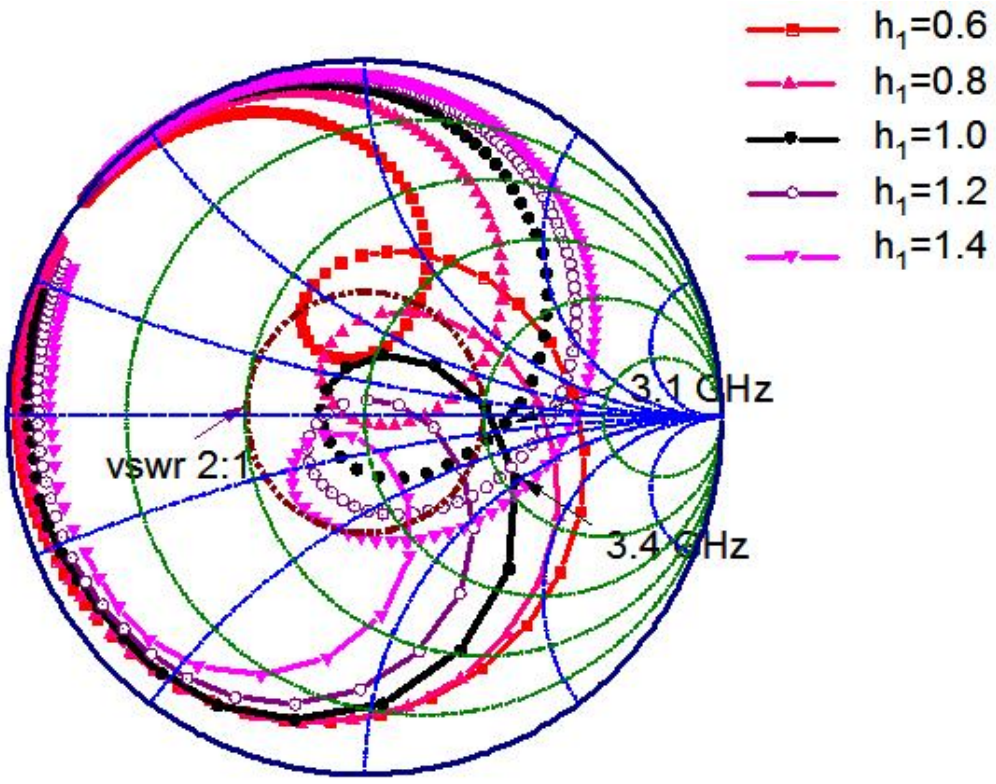


Figure 18. Smith chart of input impedance versus frequency for variable values of lower patch height at $\varepsilon_r = 3$.

## 3.4 DESIGN METHODOLOGY

Upon examination of the simulations and results presented in the last section, a major point of interest can be deduced. When stacked patch antennas were designed on LTCC Kyocera-GL550 multilayer substrate with layer thickness of 4 mils per layer, dielectric constant ($\varepsilon_r$) = 5.6, and loss tangent (tan $\delta$) = 0.0012, a relationship between the bandwidth and substrate thickness for a vertically compact structure (substrate thickness = 0.01-0.03 $\lambda_0$) is obtained. This is shown in Figure 19, where the relative 10-dB return-loss bandwidth (normalized to the resonant frequency $f_r$) is plotted as a function of the thickness of the antenna (normalized to the free-space wavelength $\lambda_0$ at $f_r$).

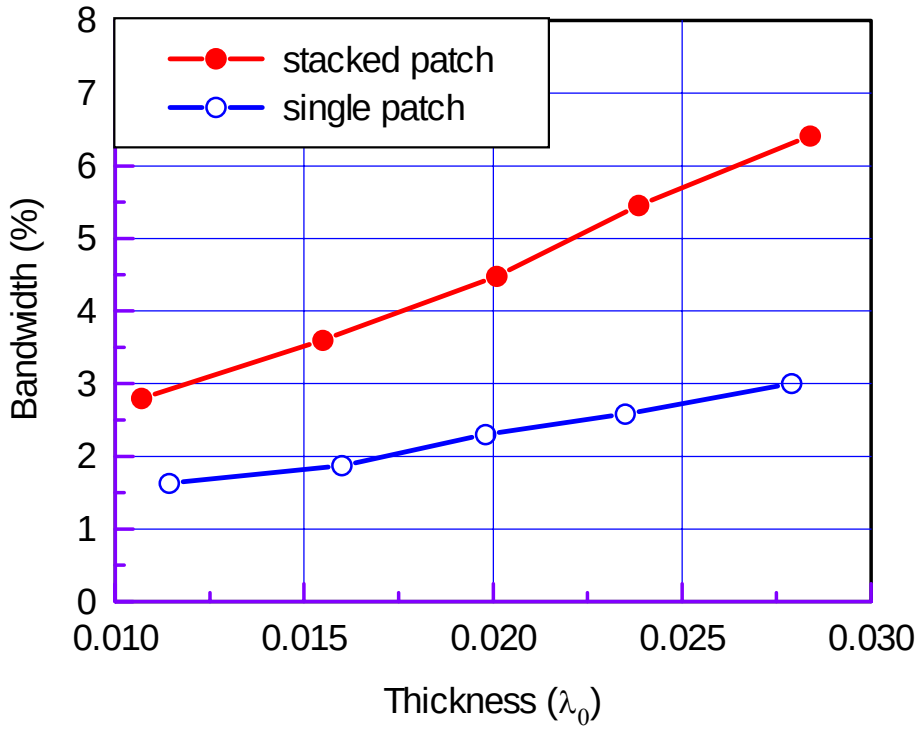


Figure 19. Impedance bandwidth versus total thickness of patch antennas on LTCC multilayer substrate.

The bandwidth of a single-patch antenna using the same type of substrate and thickness is presented in this figure as well to show the improvement in the bandwidth when using a stacked configuration. From the plot, it is observed that the compact stacked patch antenna can achieve a bandwidth of up to 7%. This is 60%-70% wider than that obtained from a single patch antenna. It is worth noting that the bandwidth of a patch antenna is mainly limited by the dielectric constant and total thickness of the substrate (i.e. the total volume occupied by the antenna). This is understandable by making note of the inversely proportional relationship between the bandwidth and the Q-factor. Moreover, a higher volumetric structure will have a lower Q-factor, and therefore, a greater bandwidth.

In lieu of this point and the results obtained last section, a set of design rules can be established for the design of stacked patch antennas on LTCC multilayer substrates with $\varepsilon_r$ and tan $\delta$ close to 5.6 and 0.0012, respectively. The steps are as follows:

Step 1: Choose an initial value for the total design thickness of the substrate h ($h = h_1 + h_2$). This thickness is usually less 0.05 $\lambda_0$ for a compact design.

Step 2: Select the lower substrate thickness, $h_1$. Through analyzing the results of many simulations using the LTCC Kyocera-GL550 multilayer, it is seen that the impedance loop will be totally inside the 2:1 vswr circle when plotted on a Smith chart, if $h_1 \approx h/4$, which is optimal for an enhanced bandwidth.

Step 3: Design the length L (which is also the width) according to the appropriate resonant frequency $f_r$ required for the application. The equation below is suggested for designing the length L:

$$L = \frac{c}{2 f_r \sqrt{\varepsilon_r}} \tag{6}$$

where all variables have been previously defined.

Step 4: Determine the upper-substrate thickness, $h_2$, for an optimal return loss. The initial value of $h_2$ can be chosen as $3h_1$ according to Step 2. The final value of $h_2$ may be obtained by simulation. Upon our observation, it is found that the impedance loop in the Smith chart will move from the upper (inductive) portion of the Smith chart to the lower (capacitive) portion as the distance between the upper patch and the lower patch is shortened. The upper substrate thickness, $h_2$, is determined when the center of the impedance loop moves closest to the center of the Smith chart, which corresponds to a minimum return loss and a better matched circuit.

Step 5: Lastly, adjust the length L slightly to cover the desired frequency band. The simulations will assist in determining the optimal length for the design.

It is possible that the optimized bandwidth of the structure is unsatisfactory for the desired application. To overcome this dissatisfaction, simply increase the lower substrate thickness, $h_1$, and repeat steps 4 and 5 until the required design specifications are met.

## 3.5 APPLICATIONS

In the final section of this chapter, the information obtained from initial simulations and analysis as well as the design rules that have been postulated will be applied to three emerging wireless communication bands. These are as follows: the 2.4 GHz ISM band, the IEEE 802.11a 5.8 GHz band, and the 28 GHz LMDS band. The substrate used in these applications is LTCC Kyocera-GL550 multilayer laminate.

A. 2.4 GHz ISM BAND

The 2.4 GHz ISM band has a 3.4% bandwidth with the center frequency, $f_c$, at 2.4415 GHz. Referring back to Fig. 8, a stacked patch antenna with a bandwidth of 3.4% should have an electrical substrate thickness of about 0.015 $\lambda_0$. The physical substrate thickness at the specified center frequency is 72 mils. At 4 mils per layer, the total requirement is 18 LTCC layers. By selecting the lower substrate thickness, $h_1$, to be ¼ the total thickness, 4 or 5 layers should be a suitable selection. By using equation (6), the length, L, is 1022 mils. The upper substrate thickness, $h_2$, can be selected through simulation. The simulated input impedance is plotted for different values of $h_2$ (in layers) on the Smith chart shown in Figure 20.

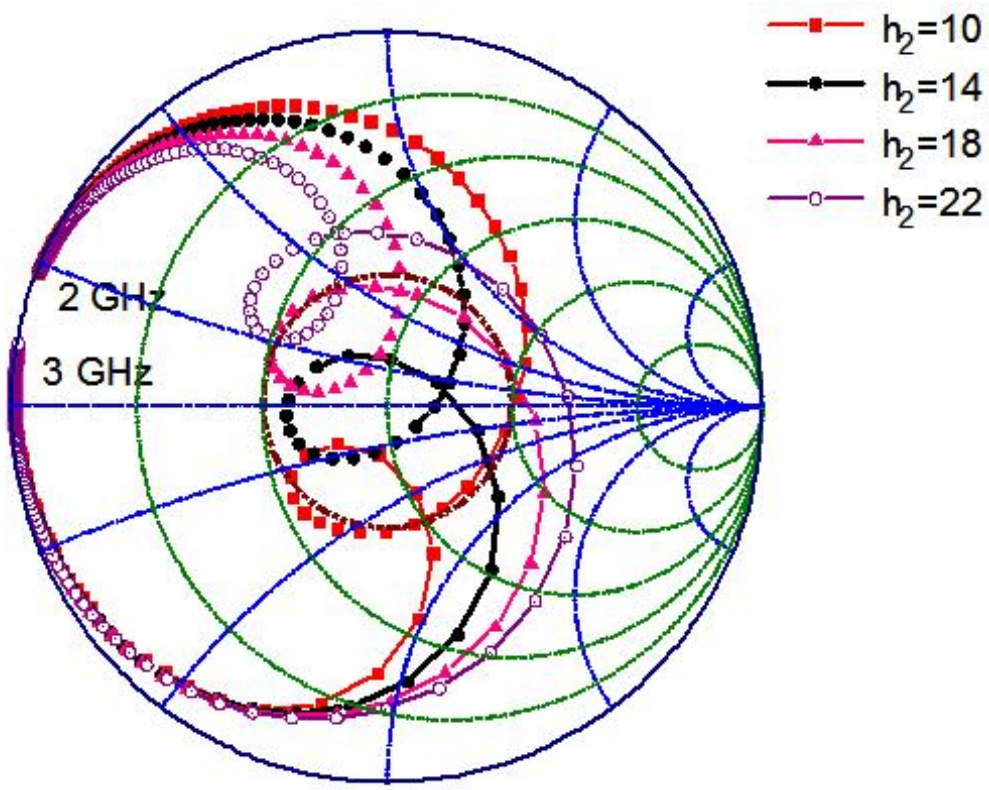


Figure 20. Smith chart of input impedance versus frequency for variable values of upper patch height at 2.4415 GHz.

It can be seen in the Smith chart that the impedance loop tends to move downward in the capacitive region as $h_2$ decreases. As explained earlier, a higher capacitance is exhibited as the lower and upper patches are closer to each other. When the impedance loop moves closest to the center of the Smith chart and the loop is totally inside the 2:1 vswr circle, a minimum return loss and an optimized bandwidth can be achieved. This is the case for $h_2$ = 14 layers. Therefore, a total substrate thickness, h, of 19 layers (not 18 layers) is necessary for an optimized bandwidth design with $h_1$ and $h_2$ equal to 5 and 14 layers, respectively. This coincides closely to the ¼ ratio of $h_1$ to h. Lastly, the antenna length, L, has to be modified to meet the band specification. Upon simulation, this value is reduced to 966 mils. The input impedance and the return loss versus frequency are plotted in Figure 21. This graph shows the two resonances that are close to each other in the return loss which contributes to a wider bandwidth.

B. IEEE802.11a 5.8 GHz BAND

A similar approach was taken for this application. The selected center frequency is around 5.8 GHz. Referring to Fig. 8, the electrical substrate thickness for this band should be approximately 0.015 $\lambda_0$. This corresponds to a physical substrate thickness of about 8 layers. Initially $h_1$ and $h_2$ is chosen to be 2 and 6 layers, respectively. Additionally, the length, L, is set at 400 mils using the formula given in step 3 of the design rules. Once again, the simulated input impedance is plotted for different values of $h_2$ (in layers) on the Smith chart that is shown in Figure 22. Coincidentally, the optimized value of $h_2$ from the Smith chart is 6 layers. This value agrees perfectly with the ¼ ratio of $h_1$ to h proposed in step 2. It is worth noting that the ¼ condition can only met for total layer thicknesses that are multiples of 4.

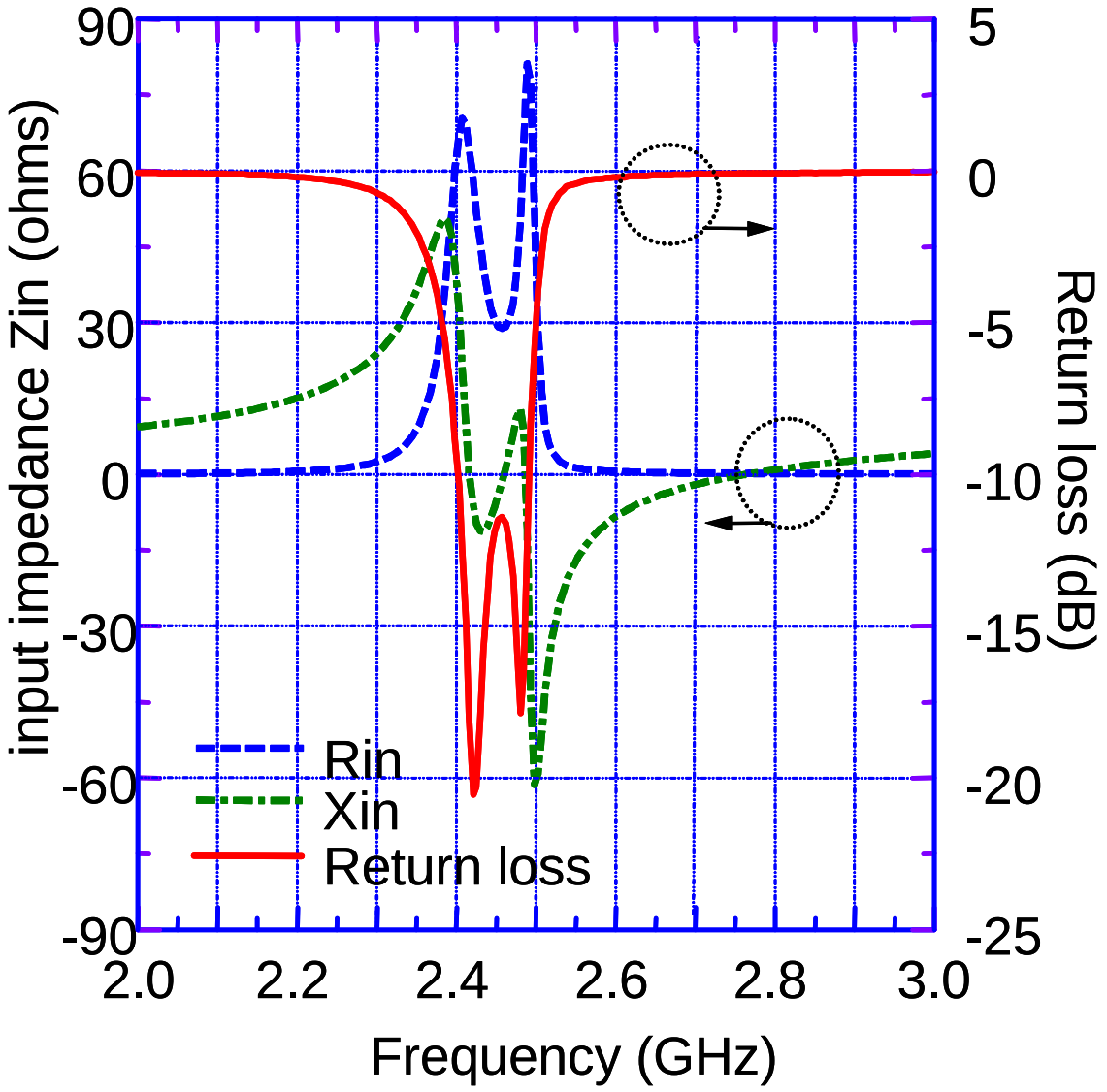


Figure 21. Input impedance and return loss versus frequency of a stacked-patch antenna at 2.4415 GHz.

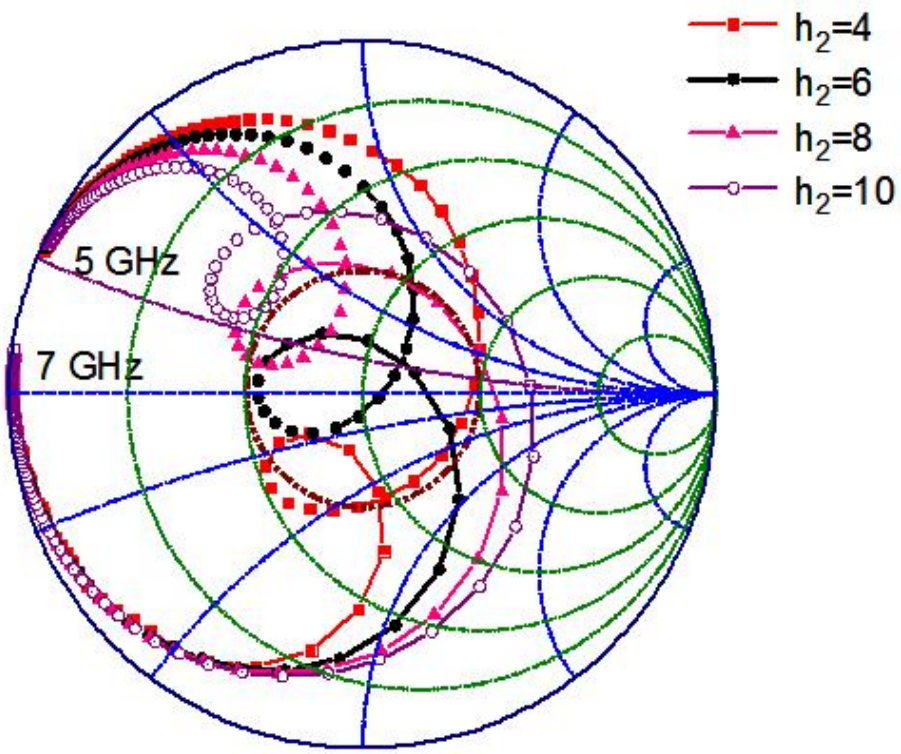


Figure 22. Smith chart of input impedance versus frequency for variable values of upper patch height at 5.8 GHz.

Figure 23 shows the simulated and measured return loss versus frequency of this structure (when $h_2$ = 6 layers) that was fabricated at Kyocera Industrial Ceramics, Corp. The measured return loss is in good agreement with the simulated results, and a bandwidth of 3.5% is observed. To measure the radiation pattern of the antenna, a modification had to be made in the feeding structure that consisted of a microstrip line connected to the lower patch with a via that passed through the substrate to the top layer and terminated to the surface of a metallic pad. The signal line of an SMA connector was then connected to the pad. The simulated and measured radiation patterns taken at 5.8 GHz are illustrated in Figure 24. The backside radiation level is about 10 dB lower than

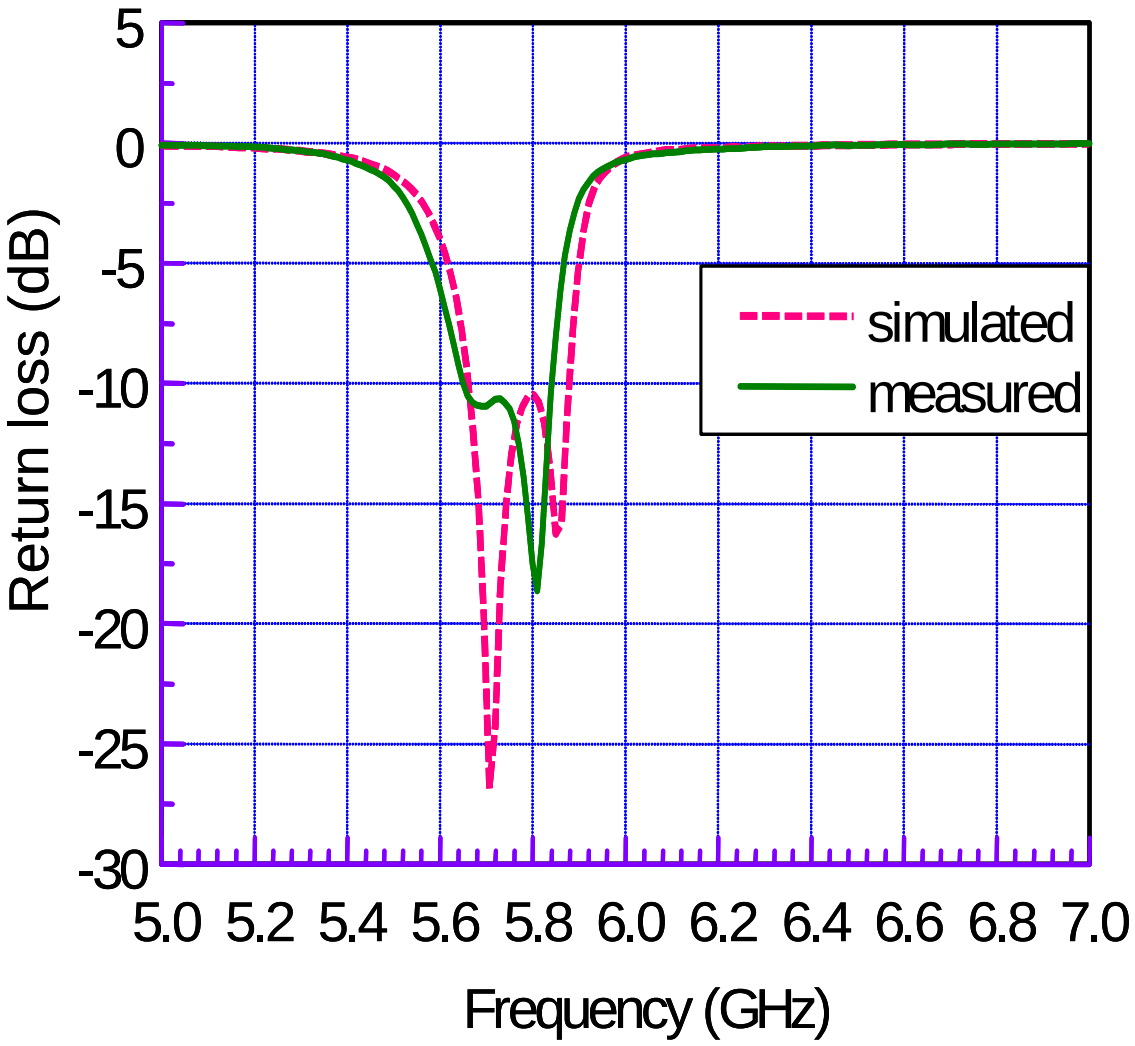


Figure 23. Return loss versus frequency of a stacked-patch antenna at 5.8 GHz.

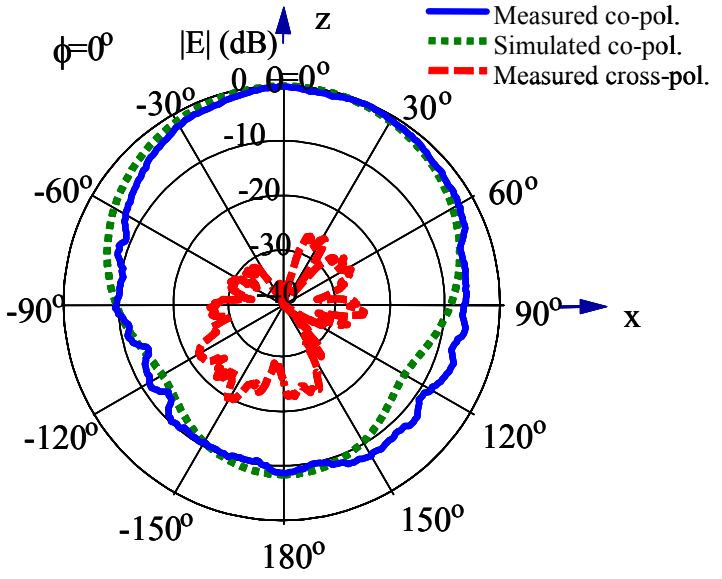


E-plane

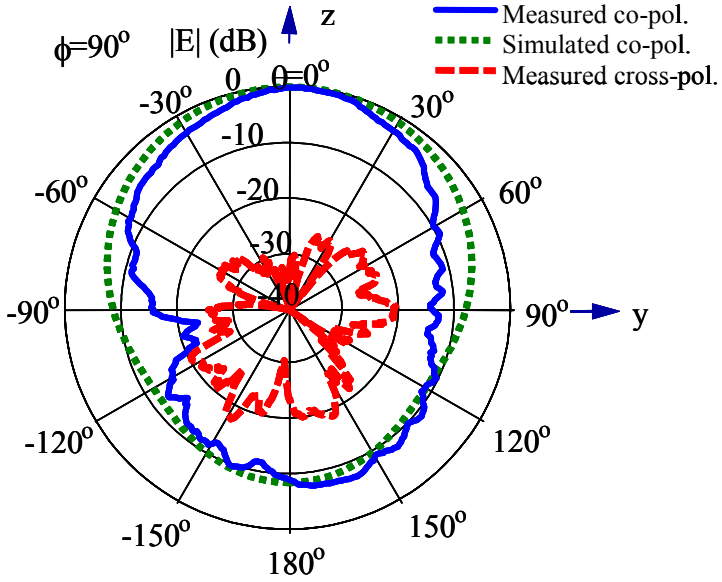


H-plane

Figure 24. Simulated and measured radiation patterns of a stacked-patch antenna at 5.8 GHz.

the maximum gain which is about 4.5 dBi. The low gain of this antenna is due to the high dielectric constant and the thin substrate thickness (0.015 $\lambda_0$). The simulated cross-polarization was less than -40 dB in the E- and H-planes, while the measured cross-polarization was less than -20 dB which is acceptable for this design. The modified feeding structure caused degradation in the cross-polarization performance of the antenna.

C. 28 GHz LMDS BAND

Once again, a similar approach was applied to the LMDS band. The required bandwidth is 7%, and the center frequency is 28 GHz. Based on Figure 19, the electrical thickness is about 0.03 $\lambda_0$ which corresponds to a physical thickness of only 3 LTCC layers due to the high operational frequency. The height, $h_1$, is chosen to be 1 layer. Due to the low number of layers that are necessary to achieve an optimal bandwidth at this frequency, the ¼ ratio rule of $h_1$ to h starts to breakdown. The simulated input impedance is plotted on the Smith chart, shown in Figure 25, for various values of $h_2$. Since this structure has a thin substrate and a fixed layer thickness, a more extreme variation will exist in the movement of the impedance loops as the value of $h_2$ changes. As is predicted by Figure 19, this value should be set at 2 layers to obtain a minimum return loss and an optimized bandwidth. The length, L, of the patch is tuned to 80 mils to fully cover the required band. The input impedance and return loss versus frequency, simulated in MicroStripes 5.5, is plotted in Figure 26 when $h_2$ = 2 layers. For comparison, the return loss versus frequency, simulated in an "in house" finite difference time domain (FDTD) code, is also shown in Figure 26. From the plots, the two simulators are in good agreement with each other. The return loss is below -15 dB for both plots. The bandwidth for both simulations is close to 7%.

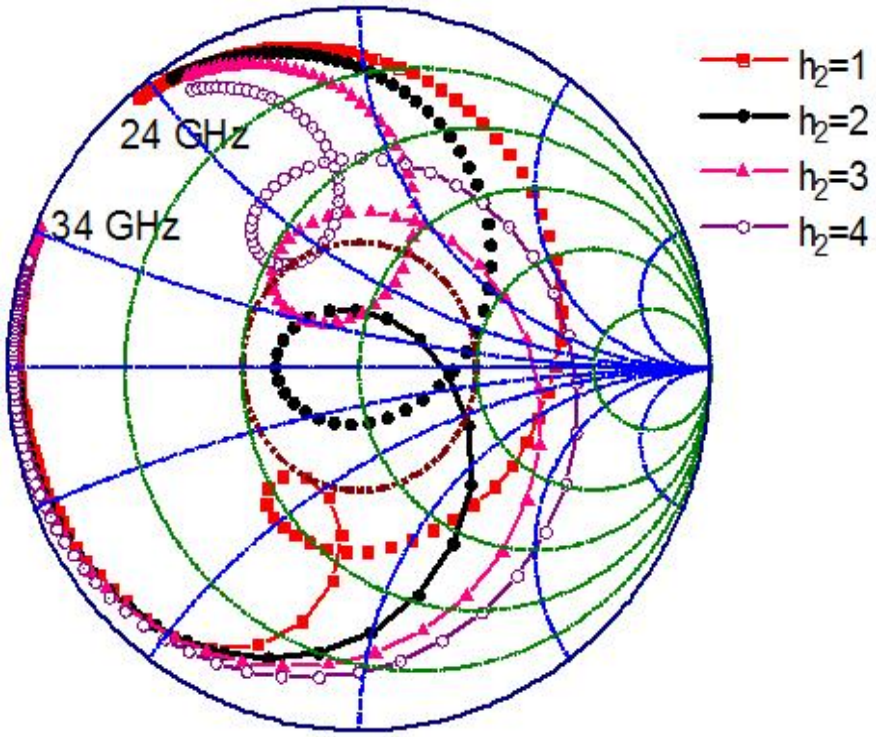


Figure 25. Smith chart of input impedance versus frequency for variable values of upper patch height at 28 GHz.

The radiation patterns for the stacked patch structure as well as a single patch with the same total thickness, h, is illustrated in Figure 27. The co-polarized (co-pol.) components of the two designs show similar performance for the E- and H-planes. The stacked patch design has a much lower cross-polarization than the single patch design. This is mainly because the single patch has a feed probe that is 4 times longer than the stacked patch structure, therefore, contributing to higher cross-polarization. All of the designs presented have a radiation efficiency greater than 85%. The power lost in these structures is due to conductor loss (conductivity, $\sigma$, equal to $5.8*10^7$ siemens per meter, S/m), dielectric loss ($\tan \delta = 0.0012$), surface wave loss ($\varepsilon_r = 5.6$), and feedline radiation. The first three types of loss are properties of the metal (copper, Cu) and the substrate.

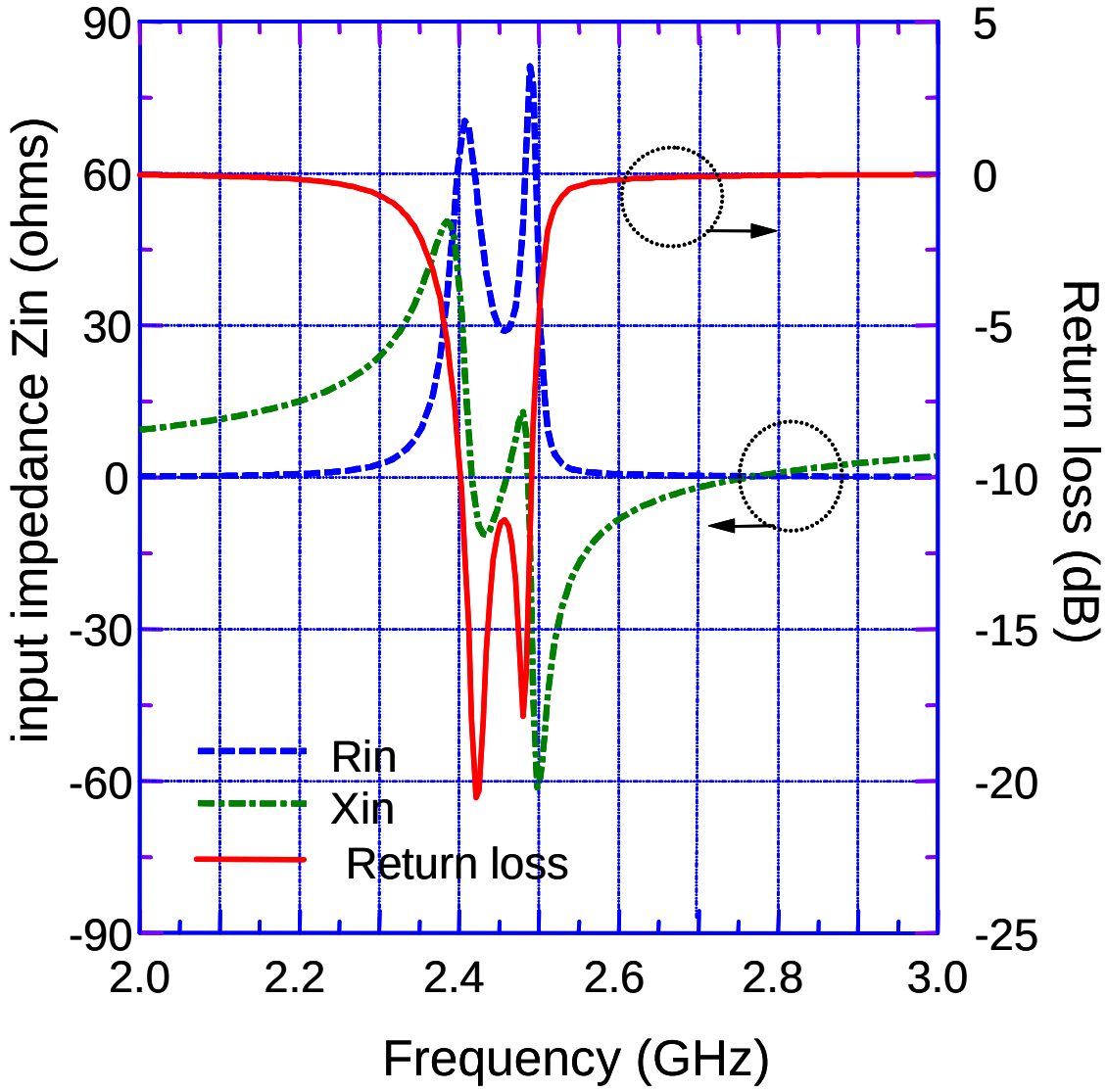


Figure 26. Input impedance and return loss versus frequency of a stacked-patch antenna at 28 GHz.

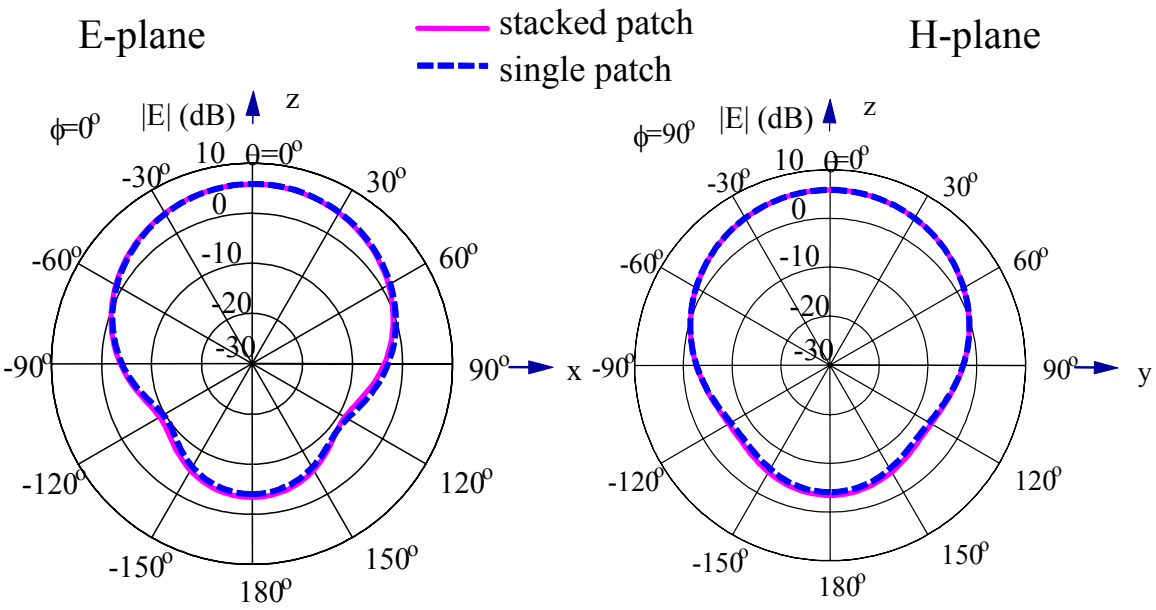


(a) co-polarized component

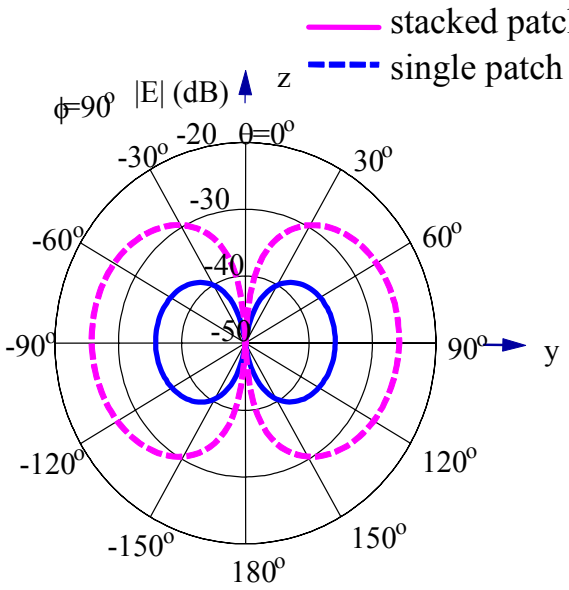


(b) cross-polarized component

Figure 27. Radiation pattern performance comparison of stacked patch versus single patch antenna at 28 GHz.

Designing thin feeding structures and transitions can circumvent the problem of feedline radiation. It is worth noting that the size of a single patch design would have to be doubled to achieve the same bandwidth as the stacked patch antenna. Therefore, the stacked patch antenna is a great solution for vertical integration of wireless transceivers using multilayer substrates such as LTCC, LCP, and multilayer organic (MLO).

# CHAPTER 4

# FOLDED SHORTED PATCH ANTENNAS

It has been previously documented that shorted patch antennas (SPAs) have a resonant length of a quarter-wavelength which, in turn, can reduce the resonant frequency by half. To optimize the level of compactness in microstrip antenna design, it is necessary to develop a design that takes two considerations into account. The first has a reduced resonant frequency that is a direct result of the reduced resonant antenna length. The second has a reduced resonant frequency that is independent of the total size of the antenna. To achieving both of these properties, many simulations and analysis will have to be done to examine the sensitivities in the design with respect to tuning the resonant of the design. Additionally, radiation pattern performance must be maintained.

## 4.1 ANTENNA STRUCTURE

The antenna structure considered in this chapter is shown in Figure 28. It consists of two square patches that are stacked for bandwidth enhancement. The dimensions of the lower patch are denoted by length, $L_1$ and width, $W_1$. Similarly, the upper patch is denoted by $L_2$ and $W_2$ for the length and width, respectively. These antennas are supported by two metal shorting walls, one for each patch that are parallel to each other (with respect to the x-axis shown in the figure) on different radiating edges. The distance between the ground plane and the lower patch is $h_1$, while that between the lower patch and the upper patch is $h_2$. The total height of the antenna (denoted by h) is the sum of these two smaller dimensions ($h_1+h_2 = h$). The substrate for this design is free space ($\varepsilon_r = 1$). This medium is favorable for designing efficient radiators with a maximal bandwidth.

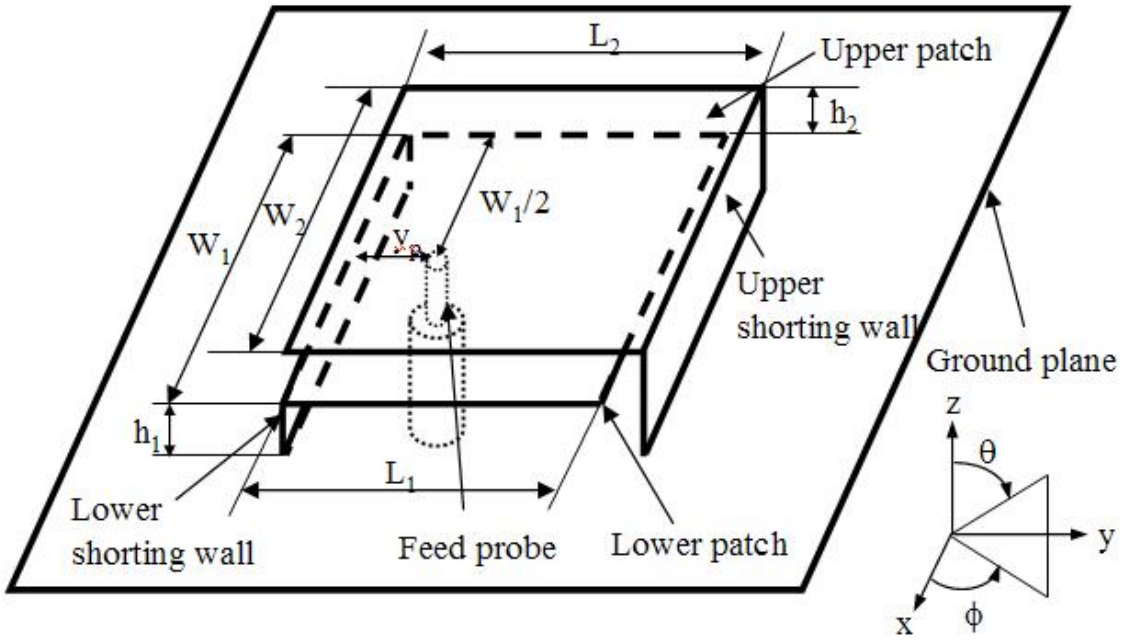


Figure 28. Antenna structure of the folded SPA.

Furthermore, placing this structure next to other components should not affect the functionality of those components due to the inexistence of the surface waves in free space. Hence, a cavity is not necessary for this design. The antenna is excited by way of a 50Ω coaxial probe where the probe's signal pin is connected to the lower patch. The charges from the lower patch electromagnetically couples energy to the upper patch which, in turn, radiates space waves. The probe is placed along the center line perpendicular to the lower patch width, $W_1$, and along a line parallel to the lower patch length, $L_1$, in order to match the 50Ω feed probe. The distance between the radiating edge of the lower patch and the feed probe is $y_p$. This parameter is varied to find the best match between the probe and antenna. The dimensions of the ground plane should be, at least, twice the size of patches to maintain compactness and prevent edge diffraction effects from degrading the radiation pattern.

## 4.2 DESIGN METHODOLOGY

The development of this structure comes from the simple design of a patch antenna. A conventional rectangular patch antenna operating at the fundamental mode ($TM_{10}$ mode) has an electrical length of $\sim\lambda_0/2$. This is illustrated in Figure 29a. If you consider that the electric field for the $TM_{010}$ mode at the middle of the patch is zero, the patch can be shorted along its middle line with a metal shorting wall without significantly changing the resonant frequency of the antenna. By doing this, the resonant length of the antenna becomes $\sim\lambda_0/4$ (shown in Figure 29b) and half of the patch can be removed. The physical length is now $L_1/2$. Then, the side of the antenna opposite the shorting wall is folded along the middle of the patch. Simultaneously, the ground plane is also folded along a position that is a short distance from the middle of the patch (Figure 29c). After this procedure, the resonant length of the antenna remains $\sim\lambda_0/4$, while the physical length is reduced by a half ($\sim\lambda_0/8$). The folding of the ground plane produces the upper patch and its shorting wall. It should be emphasized that it is necessary to fold the ground plane while folding the shorted patch. Otherwise, the folded antenna would look like an S-antenna developed in [33] for a dual-band operation. As a result of this step, the length, L1, will be slight smaller than L2 due to the small gap between the lower patch and upper patch shorting wall. Finally, a new piece of ground plane is added to the right of the existing ground plane to regenerate its original length. The new lower patch is created by pressing the two portions together. The completed structure is shown in Figure 29d. The lateral size of a conventional patch antenna has been effectively reduced from a $\sim\lambda_0/2$ to a $\sim\lambda_0/8$ structure. This is a major contribution to the goal of producing compact antennas for commercial use.

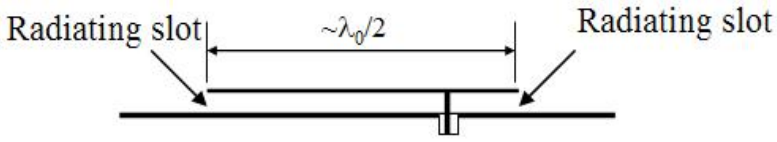


(a) conventional rectangular patch

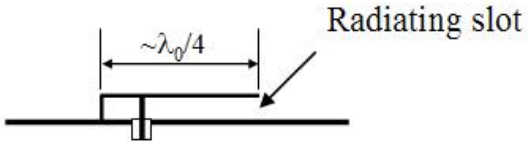


(b) conventional SPA

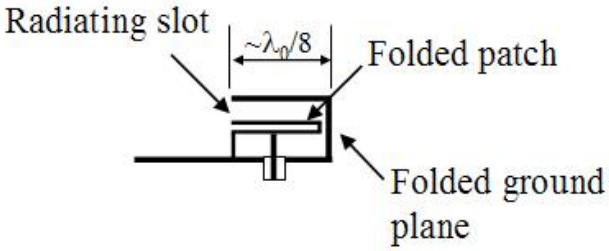


(c) folding of a conventional SPA

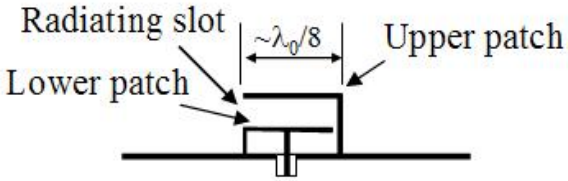


(d) folded SPA

Figure 29. Development of a folded SPA.

## 4.3 DESIGN VALIDATION

To demonstrate the potential of the design methodology proposed in the last section, two antennas were simulated using MicroStripes 5.6 (by Flomerics Ltd.) and an "in house" FDTD simulator: a standard SPA (resonant length, ~$\lambda_0/4$) and the folded SPA proposed here (resonant length, ~$\lambda_0/8$). The medium is free space. The lateral dimensions of the antennas are 10 mm x 10 mm. The patch of the standard SPA is 0.5 mm above the ground plane. For the folded SPA, the total thickness of the structure is 3 mm, and the lower patch is 0.5 mm above the ground. Figure 30 shows the return loss versus frequency for the two designs.

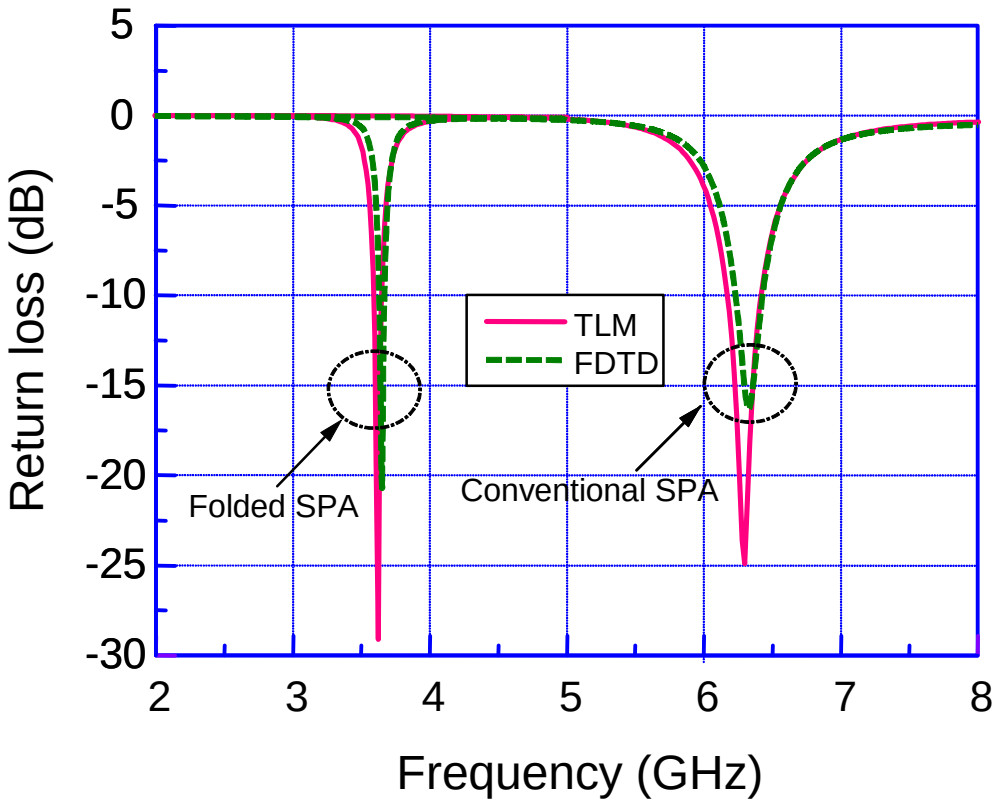


Figure 30. Return loss versus frequency of folded SPA compared to conventional SPA.

Good agreement is observed between the two simulators. The standard SPA has a resonant frequency of around 6.3 GHz, while the folded SPA resonates at approximately 3.6 GHz. Therefore, the antenna length of the folded SPA is only $\lambda_0/8$; this is about 4 times smaller than a conventional patch antenna. Additionally, these results display a resonant frequency reduction of about 43%. This is lower than the expected value of 50%. The reason for this discrepancy is due to the slight reduction in the length of the lower patch, $L_1$, (9.5 mm) needed to create the small gap between the lower patch and the shorting wall. This gap allows the power to flow from the feeding point to the radiating slot. To test this explanation, the input impedance of the folded SPA (lower patch length and width are 9.5mm and 10 mm, respectively) is plotted on the Smith chart, illustrated in Figure 31. In the same figure, the input impedance of another standard SPA is displayed. The lateral dimensions of this standard SPA are 19 mm x 10 mm. It is worth noting that the length of the standard SPA is twice as long as the folded SPA so the resonant frequency should theoretically be the same. The results from the Smith chart show that the input impedance curves are quite similar with the resonant frequency of the antennas differing by less than 3%.

Next, the near field electric fields and the surface currents for the folded SPA and the standard (19 mm x 10 mm) SPA are investigated and shown in Figure 32. It can be observed that the folded SPA has a field distribution close to that of the standard SPA. In the folded SPA, intense levels of electric fields are concentrated between the lower patch and upper patch, while similar field intensities for the standard SPA are observed opposite the shorting wall. The surface currents exhibit similar performance in examining both structures. The lower and upper surfaces of the lower patch of the folded

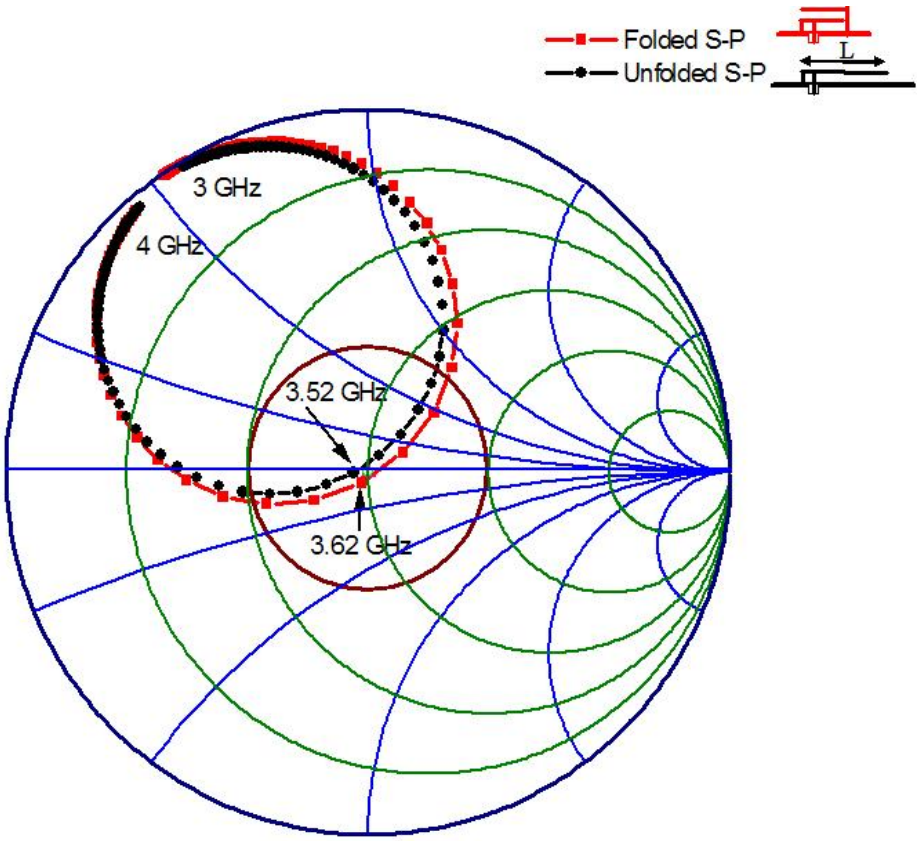


Figure 31. Smith chart of input impedance versus frequency for folded SPA and a standard SPA.

SPA correspond to the lower surface of the standard SPA. Analogously, the lower surface of the upper patch of the folded SPA corresponds to the right half-part of the ground plane beneath the standard SPA. This proves that the path of the electric fields and surface currents of the folded SPA has electrically "folded over" with the physical folding of the antenna. From the enlarged plot of the electric-field distribution in the folded SPA, an electric-field concentration between the edge of the lower patch and the shorting wall of the upper patch is observed due to the effects of a sharp edge of the lower patch and the short distance between the edge and the shorting wall. This electric-field concentration may lead to a reduction of the impedance bandwidth. One way to

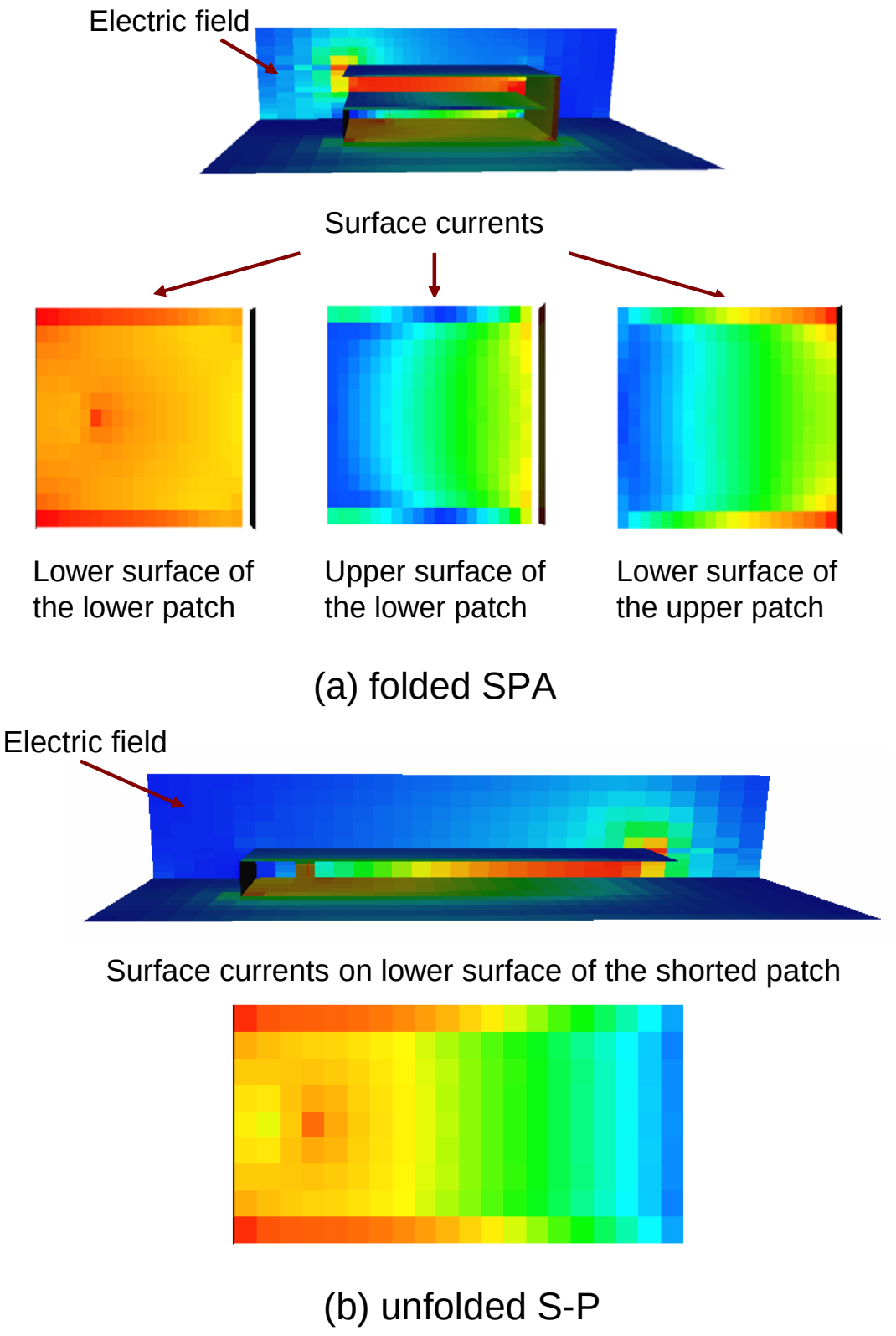


Figure 32. Electric field and surface current distributions at the resonant frequencies.

alleviate this problem would be to increase the distance between the edge and the shorting wall (decreasing length, $L_1$). However, a decrease in $L_1$ will result in an increase in the resonant frequency. For this example, the resonant frequency is 3.6 GHz with a 10-dB return-loss bandwidth of 1.9% for $L_1$ = 9.5 mm, while the resonant frequency increases to 3.8 GHz with an increased bandwidth of 2.1% when $L_1$ is decreased to 8.5 mm. The upper patch length, $L_2$, remained 10 mm for this example. The difference in the bandwidth of the folded SPA and the standard SPA is approximately 2%.

The E- and H-plane radiation pattern of the folded SPA ($f_r$ = 3.6 GHz) and the standard SPA ($f_r$ = 6.3 GHz) are presented in Figure 33. The radiating slots of both structures are oriented to the same direction. The directivity for the folded SPA (3 dB) is 1 dB lower than that of the standard SPA (4 dB) as seen in the $E_\varphi$ component. Moreover, the backside radiation level is larger for the folded SPA as well. This is due to the smaller ground plane of the antenna. A ground plane that is between 2λ - 3λ in size will have a significant effect in suppressing the backside radiation. In practice, there is a tradeoff between reducing the backside radiation (using a large ground plane) and designing a compact integrated structure (using a small ground plane). The radiation efficiencies of the standard and folded SPA are 96% and 94%, respectively. The slight reduction is a result of the strong surface current distribution on the folded SPA and the additional loss on the shorting wall of the upper patch. The metal used in the simulations was copper ($\sigma = 5.8\times10^7$ S/m).

An additional investigation was performed to further reduce the antenna's resonant length from ~$\lambda_0/8$ to ~$\lambda_0/16$. Figure 34 shows the return loss versus frequency for the 10mm x 10mm folded SPA when the lower patch is vertically placed at five

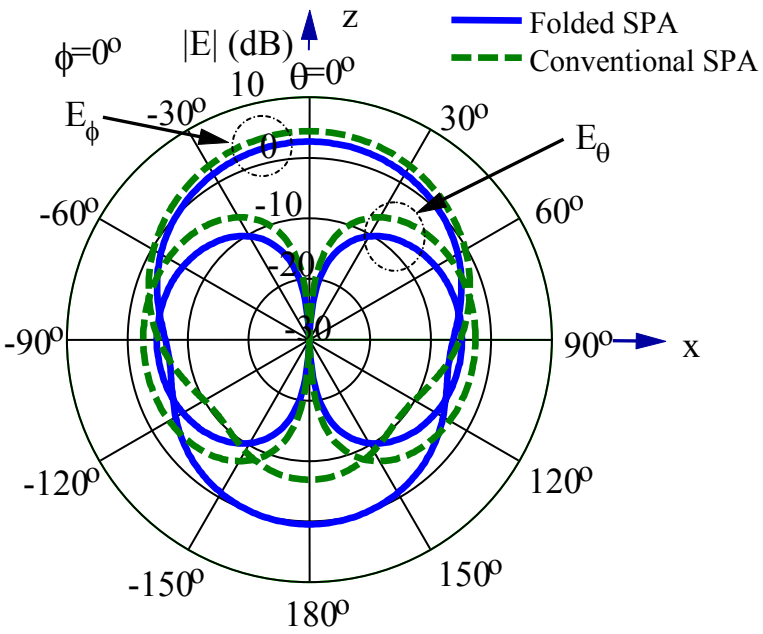


E-plane

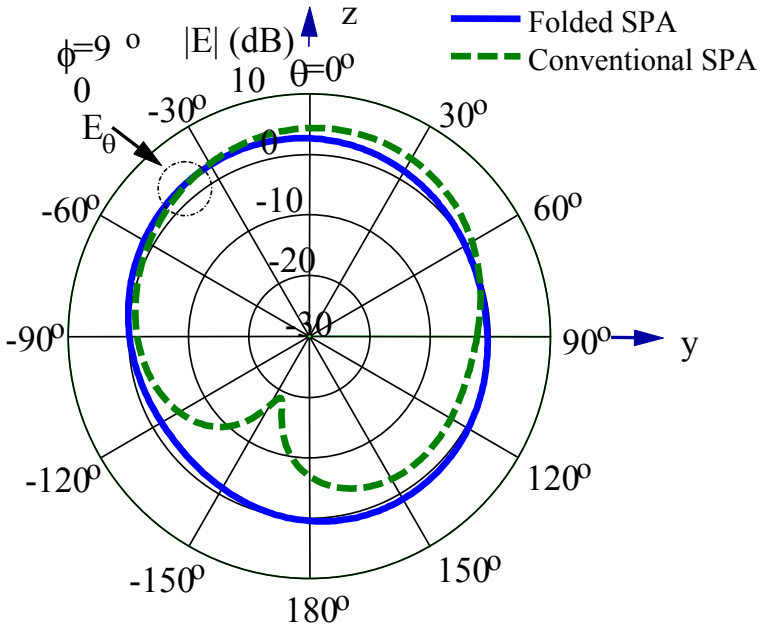


H-plane

Figure 33. Radiation patterns of folded SPA and standard SPA at 3.6 GHz.

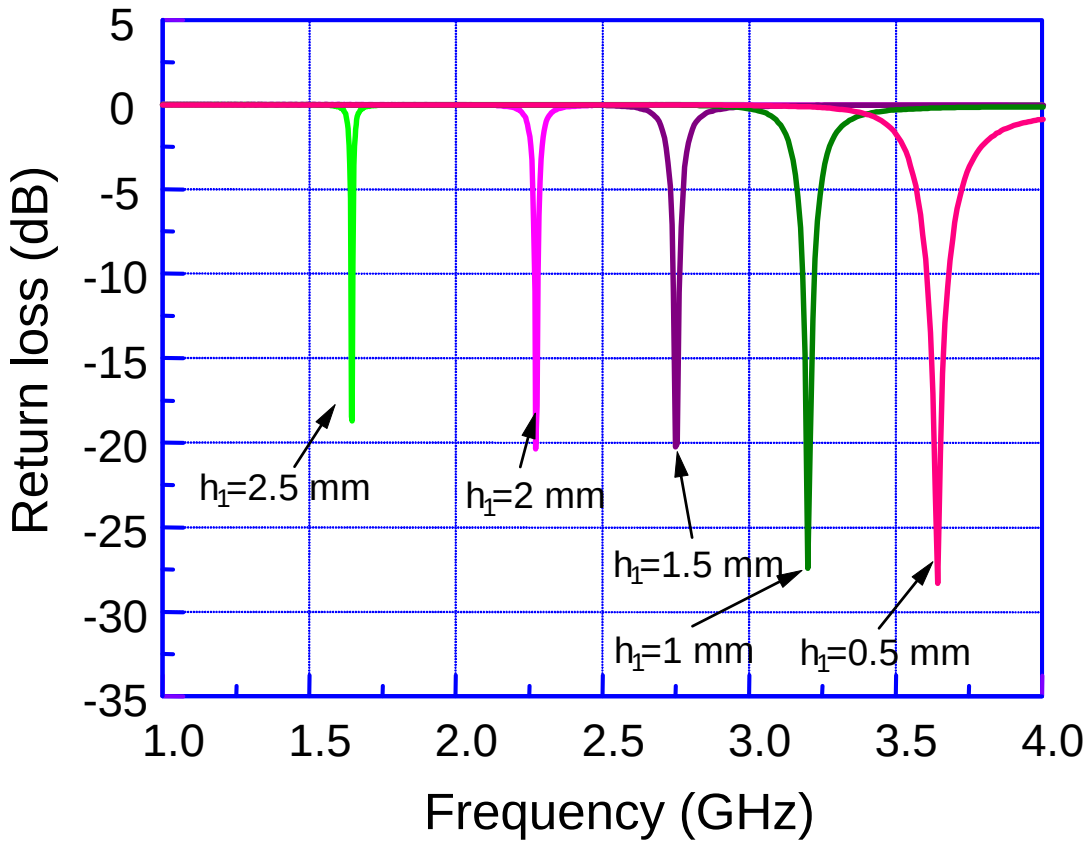


Figure 34. Return loss versus frequency for different vertical placements of lower patch.

positions between the ground plane and the upper patch. The total thickness remains 3 mm. There is a definite relationship between the lower patch height and the resonant frequency. As the height is increased, the resonant frequency is greatly reduced. By placing the lower patch 2.5 mm above the ground plane, the resonant length of the antenna can be transformed from $\sim\lambda_0/8$ to $\sim\lambda_0/16$. There is a major setback for this approach. As the upper and lower patches become closer to each other, the radiation efficiency is greatly affected. Again, this is due to the strong coupling between the plates.

For a folded SPA with an antenna length of ~$\lambda_0/16$, the radiation efficiency is less than 40%. Careful attention must be maintained when adjusting this parameter.

## 4.4 THEORETICAL ANALYSIS

Some insight on the equations and theoretical justifications that govern the proposed design are presented in this section. In order to avoid repetition and confusion, the author has decided to utilize the theoretical analysis presented in [34], written by G. DeJean, R. L. Li, M. M. Tentzeris, and J. Laskar.

The impedance performance of the folded SPA antenna can be analyzed by employing a simple transmission-line model. Consider a folded SPA with three different patch-height arrangements: case 1 ($h_1 = h_2 = 1.0$ mm), case 2 ($h_1 = 0.5$ mm, $h_2 = 1.0$ mm), and case 3 ($h_1 = 1.0$ mm, $h_2 = 0.5$ mm). The equivalent standard SPA configurations associated with these three cases are illustrated in Figure 35a-35c. By neglecting the effect of discontinuities because $|h_1 - h_2|$ is much smaller (at least ten times less) than the length of the folded SPA, the standard SPA can be represented by a transmission-line equivalent circuit as shown in Figure 35d with input impedance

$$Z_{in} = jX_f + Z_1 \tag{7}$$

where $X_f$ is the feed-probe reactance given by

$$X_f = \frac{\omega\mu_0 h_1}{2\pi}\left[\ln\left(\frac{2}{\beta * r_p}\right) - 0.57721\right] \tag{8}$$

with $\beta = 2\pi / \lambda_o$ and $r_p$ is the feed-probe radius. $Z_1$ (= $1/Y_1$) is obtained from the transmission-line equivalent circuit, that is,

$$Y_1 = Y_{01} \frac{1}{j \tan(\beta y_p)} + Y_{01} \frac{Y_2 + jY_{01} \tan\left[\beta(L_1 - y_p)\right]}{Y_{01} + jY_2 \tan\left[\beta(L_1 - y_p)\right]} \tag{9}$$

and

$$Y_2 = Y_{02} \frac{Y_s + jY_{02} \tan(\beta L_1)}{Y_{02} + jY_s \tan(\beta L_1)} \tag{10}$$

where $Y_{01}$ and $Y_{02}$ are respectively the characteristic admittances of the lower and upper patches, and $Y_s = G_s + jB_s$.

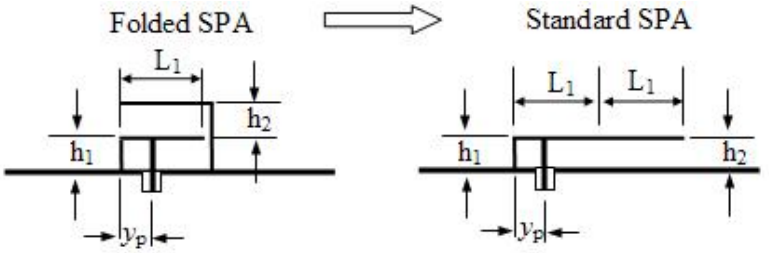


(a) case 1 ($h_1$=$h_2$=1.0 mm)

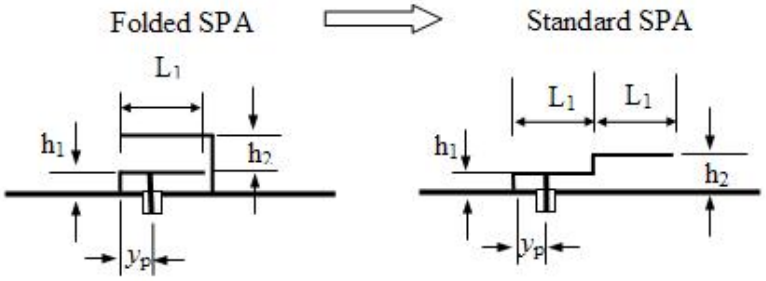


(b) case 2 ($h_1$=0.5 mm, $h_2$=1.0 mm)

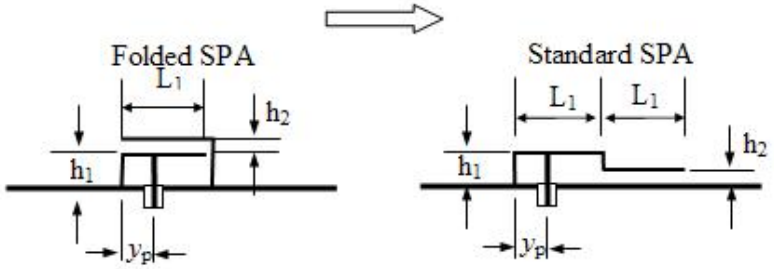


(c) case 3 ($h_1$=1 mm, $h_2$=0.5 mm)

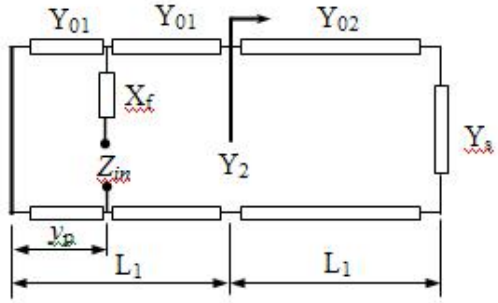


(d) simple transmission-line model

Figure 35. Folded SPA and its equivalent transmission-line model.

Here, $G_s$ is the conductance associated with the power radiated from the radiating edge (or the radiating slot), and $B_s$ is the susceptance due to the energy stored in the fringing field near the edge. In our calculations, we used the following equations for $Y_0$ (= $Y_{01}$ for $h = h_1$ or $Y_{02}$ for $h = h_2$), $G_s$, and $B_s$

$$Y_0 = \frac{W/h + 1.393 + 0.667\ln(W/h + 1.444)}{120\pi} \quad \text{for } W/h \geq 1 \tag{11}$$

$$G_s = \begin{cases} W^2/(90\lambda_0^2) & for \quad W \leq 0.35\lambda_0 \\ W/(120\lambda_0) - 1/(60\lambda_0^2) & for \quad 0.35\lambda_0 \leq W \leq 2\lambda_0 \quad (h_2 \leq 0.02\lambda_0) \\ W/(120\lambda_0) & for \quad 2\lambda_0 \leq W \end{cases} \tag{12}$$

$$B_s = Y_{02}\tan(\beta\Delta l) \tag{13}$$

$$\Delta l = \frac{\varsigma_1\varsigma_3\varsigma_5}{\varsigma_4} h_2 \tag{14}$$

where W is the width of the patch and coefficients $\zeta_1$, $\zeta_3$, $\zeta_4$, $\zeta_5$ can be found in Appendix B of [4].

The theoretical results for the input impedance have been obtained using the above analytical expressions and compared in Figure 36 with numerical simulation (using Micro-Stripes 5.6) for the above three cases of the folded SPA, demonstrating a good agreement. The difference between the theoretical and simulated resonant frequencies is less than 3%. It can be observed that the resonant frequency decreases as $h_2/h_1$ decreases. For simplicity, we neglect the effects of $Y_s$ (typically $Y_s << Y_0$) and $X_f$ (note that we are

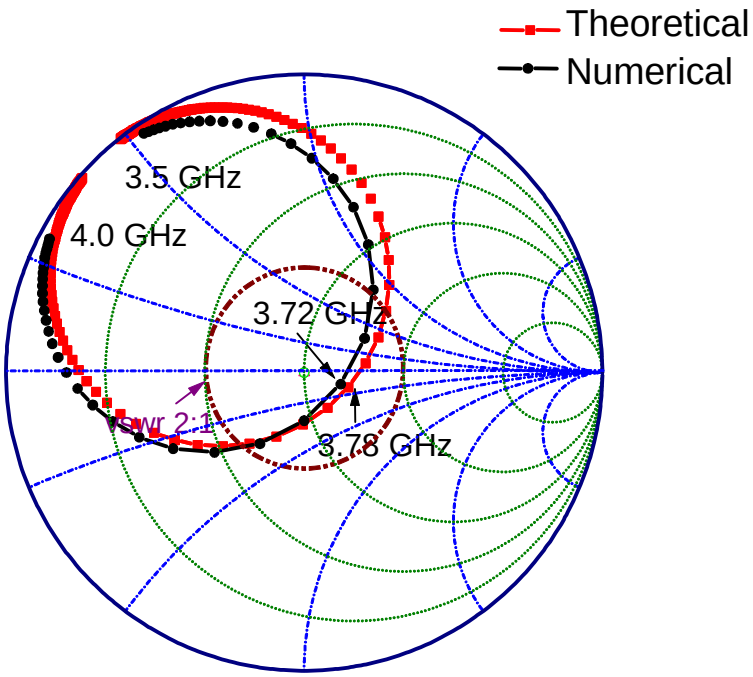


(a) case 1 ($h_1$=$h_2$=1.0 mm)

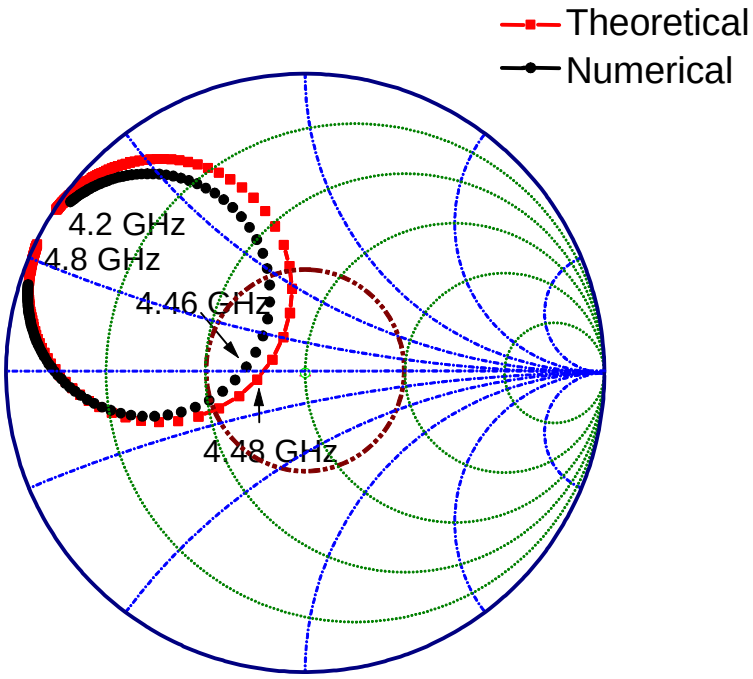


(b) case 2 ($h_1$=0.5 mm, $h_2$=1.0 mm)

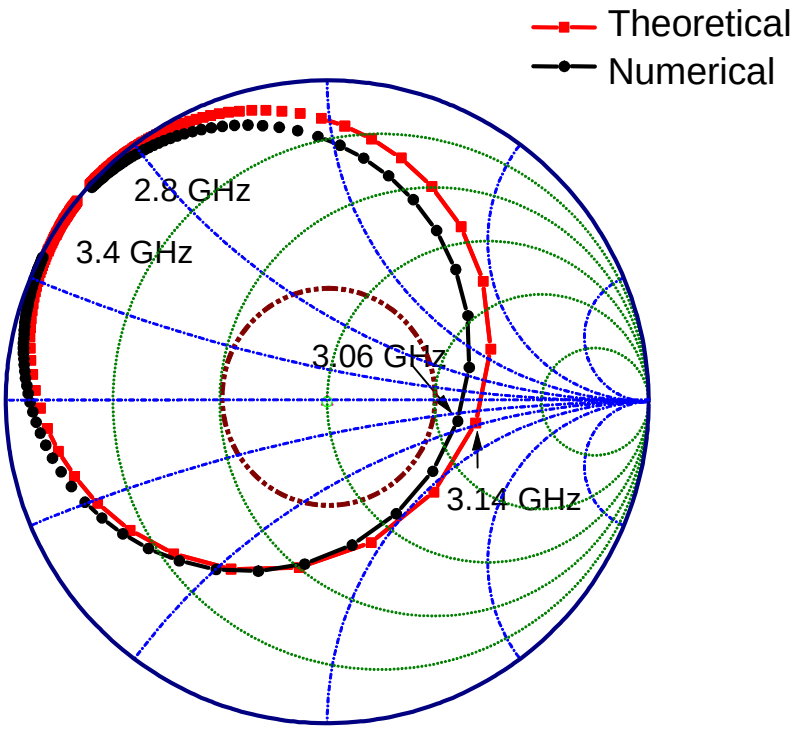


(c) case 3 ($h_1$=1.0 mm, $h_2$=0.5 mm)

Figure 36. Smith chart of input impedance versus frequency for cases 1-3.

now only interested in the resonance of the patch alone). As a result the standard SPA becomes a shorted transmission line loaded with an open transmission line. Assuming that the resonant frequency is almost independent on the feeding position, we can choose $y_p = L_1$. Thus, $Y_1$ becomes

$$Y_1 = Y_{01}\frac{1}{j\tan(\beta L_1)} + jY_{02}\tan(\beta L_1) \tag{15}$$

At resonance, $Y_1 = 0$ leads to

$$Y_{01}/\tan(\beta L_1) = Y_{02}\tan(\beta L_1) \text{ or } \tan(\beta L_1) = \sqrt{Y_{01}/Y_{02}} \tag{16}$$

From (11), it is observed that $Y_0$ is inversely proportional to h; therefore, we can find from (16) that the resonant frequency varies proportionally with $h_2/h_1$. A graphical solution of (16) for resonant frequency is depicted in Figure 37, where the intersection of the curves

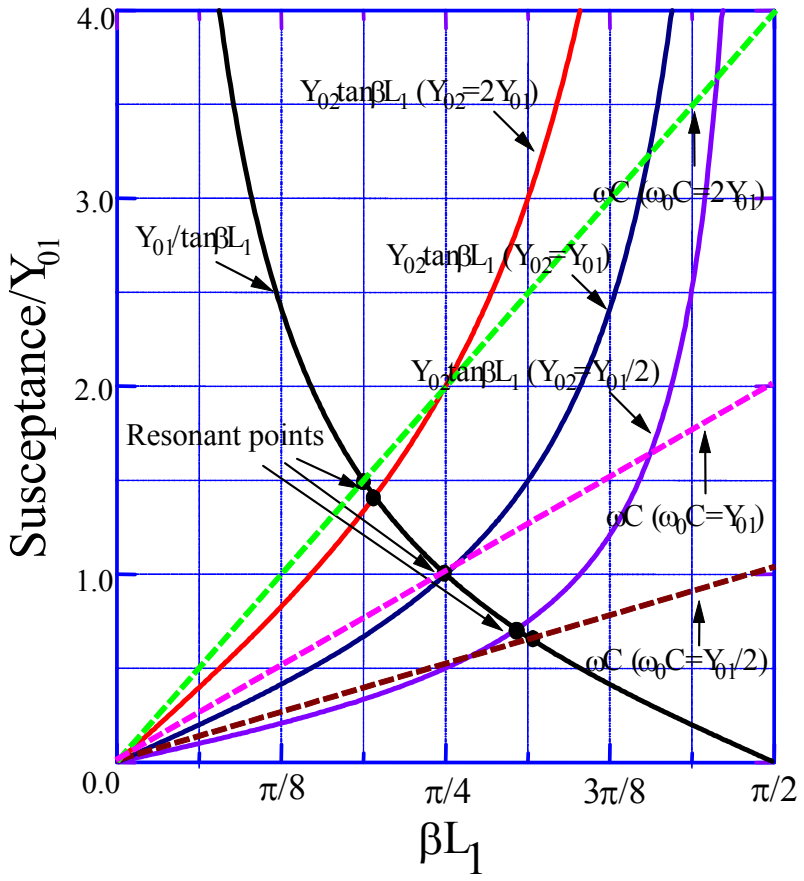


Figure 37. Graphical solution of Equations (10) and (11) for the calculation of the resonant frequencies of a capacitively loaded S-P ( $\omega_0 = 3\pi/(4L_1)\times 10^8$ rad/sec)

$Y_{01}$ / tan ($\beta L_1$) and $Y_{02}$ / tan($\beta L_2$) implies a resonant point. Observe that if $Y_{01} = Y_{02}$, then $\beta L_1 = \pi/4$, which corresponds to an antenna length of $L_1 = \lambda_0/8$. Also observe that an increase in $Y_{02}$ leads to a decrease in $\beta L_1$ if $Y_{01}$ keeps unchanged. Considering the upper

patch as a capacitive load leads to a clear picture of the physical insight for the above analysis. Replacing the upper patch with a capacitor C which is connected between the radiating edge of the lower patch and the ground plane, (15) becomes

$$Y_{01} / \tan(\beta L_1) = \omega C \ . \tag{17}$$

A graphical solution of (17) is also plotted in Figure 37. Obviously, the resonant frequency decreases as the capacitance increases. The resonant length of a capacitively loaded SPA will reduce to $L_1 = \lambda_0/8$ if the loaded capacitance is $C = Y_{01}/\omega_o$, where $\omega_o = 3\pi / (4L_1) \times 10^8$ radians/second (rad/sec) obtained from $\beta L_1 = \pi/4$. Actually a decrease in $h_2$ is equivalent to an increase in the coupling capacitance between the upper and lower patches, thus eventually leading to a decrease in the resonant frequency. In fact, some of small antenna structures can be considered as a capacitively loaded patch.

It has to be noted that the above simple transmission-line model works well only if the total height of the folded patch is much smaller (at least five times less) than the patch length and if the discontinuity ($|h_1 - h_2|$) is much shorter (at least 10 times less) than the total length of the folded patch antenna.

## 4.5 APPLICATIONS

A practical design of a folded SPA has been constructed and simulated to operate in the 2.4 GHz ISM band. Although he patch dimensions are 15 mm x 15 mm ($\sim\lambda_0/8$ x $\sim\lambda_0/8$), the upper patch is slightly greater in order to create the gap between the lower patch and the upper shorting wall necessary to maintain the path of electric fields. The antenna (fed by coaxial probe) is positioned 5 mm from the lower shorting wall. The total thickness is 6 mm. The lower patch is elevated 2.85 mm above the ground plane.

This placement allows the resonant frequency to be tuned to 2.44 GHz. This antenna was fabricated by Georgia Tech Research Institute (GTRI), and measurements were taken. The finished prototype is shown in Figure 38. The simulated and measured return loss versus frequency is illustrated in Figure 39. Good agreement is observed in the two plots. The slight frequency shift is primarily due to a dimensional inaccuracy in the fabrication.

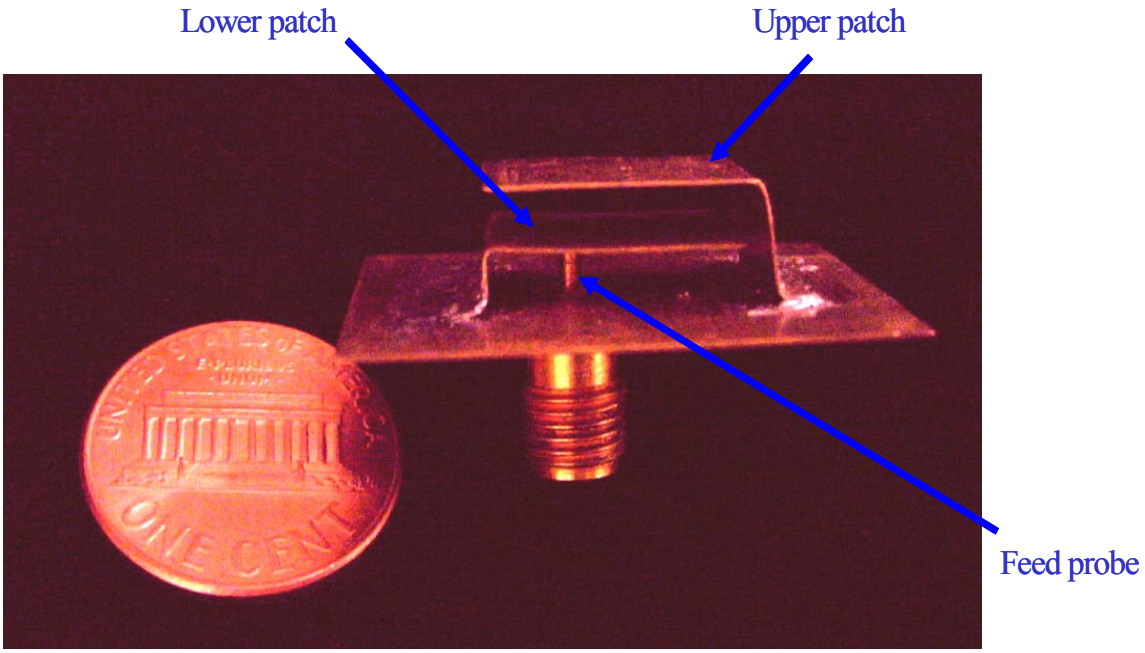


Figure 38. Prototype of folded SPA at 2.4 GHz.

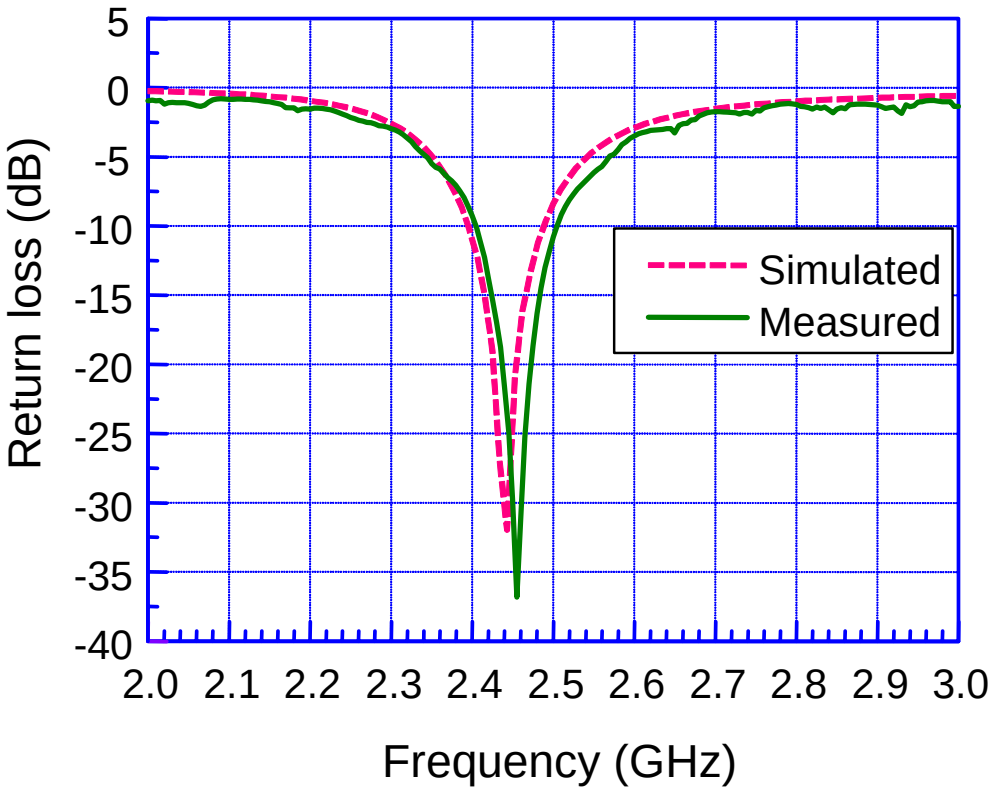


Figure 39. Return loss versus frequency of folded SPA at 2.4 GHz.

The radiation patterns for the E- and H-plane are displayed in Figure 40. Once again, good agreement is seen in the $E_\theta$ and $E_\varphi$ components. The high levels of backside radiation are due to the existence of a small ground plane (30mm x 30mm) with respect to the patch dimensions. This can be improved by implementing a compact periodic bandgap (PBG) or soft-and-hard surface (SHS) structure.

As a point of interest, the folded SPA can be designed using a multilayer substrate such as LTCC or LCP. In order to integrate this antenna into a multilayer package, the shorting walls would be replaced by rows of vias. The via-to-via spacing is a critical parameter to control. Spacing the vias too far from each other will have no significant effect in keeping the electric fields confined under the lower and upper patches. On the

other hand, an extremely close spacing will cause some parasitic capacitance and additional currents from the vias that may affect the return loss and reduce the efficiency of the antenna. Additionally, the probe would be replaced by a via that passes through the ground plane and terminates on the top of a microstrip line. A complete analysis (through simulation and theory) is necessary to effectively design this structure to be integrated into a compact 3D module.

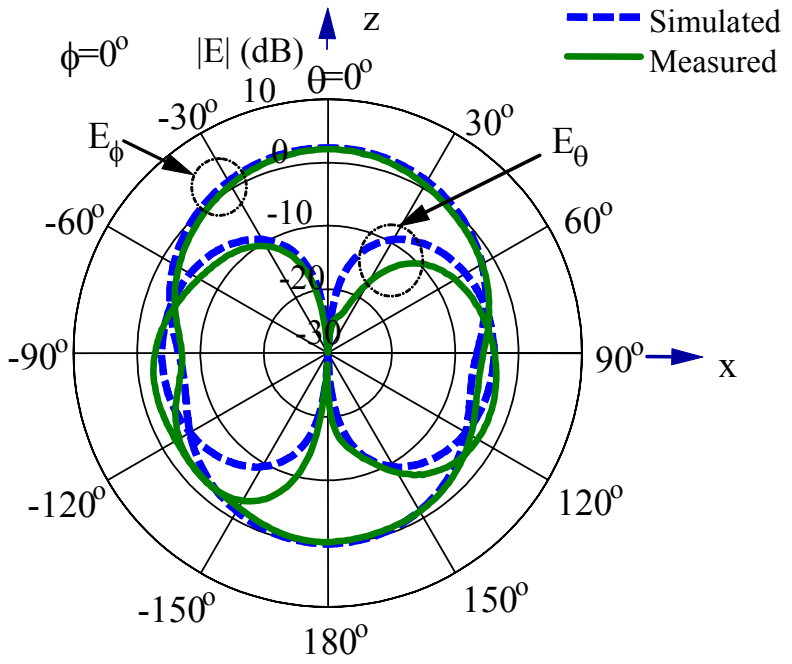


E-plane

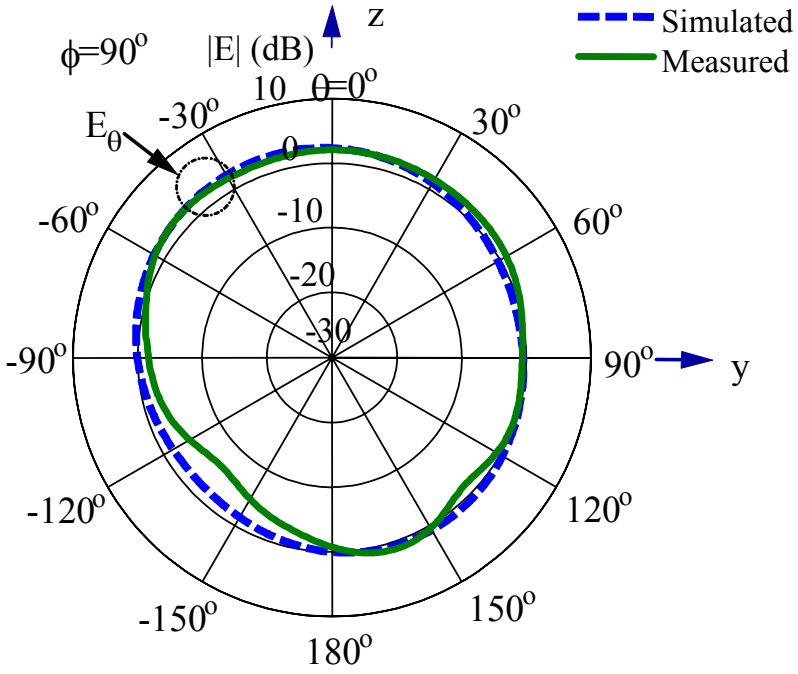


H-plane

Figure 40. Radiation patterns of folded SPA at 2.4 GHz.

# CHAPTER 5

# CONCLUSION

The goal of this thesis has been to develop and optimize two compact planar antenna architectures for various wireless communication applications and frequency bands. The design process analysis of these architectures that can be implemented into a multilayer package for the development of integrated wireless 3D modules has been presented. Although these antennas are compact in size, the full functionality and performance capability of these designs have not been compromised. In fact, these designs show some performance improvement, such as a lower cross-polarization. A thorough analysis of the theoretical performance, the schematic of the antenna structure, and the simulated and measurement results has been performed. From this analysis, it has been concluded that two successful compact antenna designs have been introduced to the wireless and radio frequency design community.

First, compact stacked patch antennas using LTCC multilayer technology have been presented. A rigorous trial and error investigation has been performed that addresses most of the critical parameters that can affect the design. The major focus of this investigation has been the variance of the impedance response versus frequency as the dielectric constant and the placement of the lower and upper patches are changed. From this initial analysis, a set of design rules has been established for the purpose of designing optimized bandwidth compact antennas on LTCC multilayer substrates. To verify its effectiveness, the proposed design rules have been applied to three emerging wireless bands: the 2.4 GHz ISM band, the IEEE 802.11a 5.8 GHz band, and the 28 GHz LMDS band. It has been observed that the return loss and the impedance bandwidth are

optimized for all three bands. A maximum bandwidth of 7% in contrast to single patch's 4% has been achieved for an antenna operating in the LMDS band. The radiation patterns exhibit a similar performance in comparison to a single patch antenna, though the cross-polarization levels have been significantly reduced, something that could enable the use of this antenna to 3G or mm-wave polarization-diversity systems. The derived design rules provide a detailed guide to constructing multilayer stacked patch antennas on LTCC or other organic (e.g. LCP, BCB) multilayer laminates that can be easily integrated with vertically integrated modules for a variety of frequency bands up to mm-wave range.

The second antenna architecture that has been thoroughly investigated concerns the folded shorted patch antennas (SPAs) that can be easily implemented to significantly reduce the resonant frequency of a standard patch antenna. The design methodology of this structure starts with a conventional half-wave (~$\lambda_0$/2). From there, placing a metal wall along the middle line of the patch with a metal shorting wall reduces the resonant length to ~$\lambda_0$/4. Then, a folding procedure that includes folding the ground and the patch simultaneously further reduces the resonant length to ~$\lambda_0$/8. Upon completing this step, varying the height of the lower patch can result in as much as a ~$\lambda_0$/16 resonant length. A comparison between a folded SPA and a standard SPA has validated the folding technique proposed in this document. Additionally, a theoretical analysis has been presented to justify the design methodology. Finally, the folded SPA has been applied to the 2.4 GHz ISM band and can be easily extended to higher frequencies especially for ceramic or organic substrates. The measured results have closely verified those obtained via simulation. The folded SPA can be implemented into 3D packages for wireless, automotive or miniaturized sensor applications.

# APPENDIX A

## LIST OF PUBLICATIONS


1. E. Tentzeris, R. L. Li, K. Lim, M. Maeng, E. Tsai, G. DeJean, J. Laskar, " Design of compact stacked-patch antennas on LTCC technology for wireless communication applications," IEEE Antennas and Propagation Society International Symposium, Volume: 2, June 2002, pp. 500-503.

2. R. L. Li, K. Lim, M. Maeng, E. Tsai, G. DeJean, M. M. Tentzeris, J. Laskar, "Design of Compact Stacked-Patch Antennas on LTCC Technology for Wireless Communication Applications," IEEE Antennas and Propagation Society International Symposium, Volume: 4, June 2002, pp. 26-29.

3. R. L. Li, G. DeJean, M. M. Tentzeris, J. Laskar, "Integration of Miniaturized Patch Antennas with High Dielectric Constant Multilayer Packages and Soft-and-Hard Surfaces (SHS)" IEEE Electronic Components and Technology Conference, May 2003, pp. 27-30.

4. R. L. Li, G. DeJean, M. M. Tentzeris, J. Laskar, J. Papapolymerou, "LTCC multilayer based CP patch antenna surrounded by a soft-and-hard surface for GPS applications," IEEE Antennas and Propagation Society International Symposium, Volume: 2, June 2003, pp. 651-654.

5. R. L. Li, G. DeJean, M. M. Tentzeris, J. Laskar, "Novel multi-band broadband planar wire antennas for wireless communication handheld terminals," IEEE Antennas and Propagation Society International Symposium, Volume: 3, June 2003, pp. 44-47.

6. R. L. Li, G. DeJean, M. M. Tentzeris, J. Laskar, V. F. Fusco, R. Cahill, "Unidirectional printed loop antenna," IEEE International Symposium on Antennas, Propagation and EM Theory, Nov. 2003, pp. 104-107.

7. R. L. Li, G. DeJean, M. M. Tentzeris, J. Laskar, "Development and analysis of a folded shorted-patch antenna with reduced size," IEEE Transactions on Antennas and Propagation, Volume: 52, Issue: 2, Feb. 2004, pp. 555-562.

8. R. L. Li, G. DeJean, M. M. Tentzeris, J. Papapolymerou, J. Laskar, "FDTD analysis of patch antennas on high dielectric-constant substrates surrounded by a soft-and-hard surface," IEEE Transactions on Magnetics, Volume: 40, Issue: 2, March 2004, pp. 1444-1447.

9. M. M. Tentzeris, J. Laskar, J. Papapolymerou, S. Pinel, V. Palazzari, R. L. Li, G. DeJean, N. Papageorgiou, D. Thompson, R. Bairavasubramanian, S. Sarkar, J. H. Lee, "3-D-integrated RF and millimeter-wave functions and modules using liquid crystal polymer (LCP) system-on-package technology," IEEE Transactions on Advanced Packaging, Volume: 27 , Issue: 2 , May 2004, pp. 332-340.

10. V. Palazzari, D. Thompson, N. Papageorgiou, S. Pinel, J. H. Lee, S. Sarkar, R. Pratap, G. DeJean, R. Bairavasubramanian, R. L. Li, M. M. Tentzeris, J. Laskar, J. Papapolymerou, L. Roselli, "Multi-band RF and mm-wave design solutions for integrated RF functions in liquid crystal polymer system-on-package technology" IEEE Electronic Components and Technology Conference, Volume: 2, June 2004, pp. 1658-1663.

11. R. L. Li, G. DeJean, M. M. Tentzeris, J. Laskar, "Integrable miniaturized folded antennas for RFID applications" IEEE Antennas and Propagation Society International Symposium, Volume: 2, June 2004, pp. 1431-1434.

12. G. DeJean, M. M. Tentzeris, "Modeling and optimization of circularly-polarized patch antennas using the lumped element equivalent circuit approach" IEEE Antennas and Propagation Society International Symposium, Volume: 4, June 2004, pp. 4432-4435.

13. G. DeJean, R. L. Li, M. M. Tentzeris, J. Papapolymerou, J. Laskar, "Radiation-pattern improvement of patch antennas using a compact soft/hard surface (SHS) structure on LTCC multilayer technology," IEEE Antennas and Propagation Society International Symposium, Volume: 1, June 2004, pp. 317-320.

14. R. L. Li, G. DeJean, M. Maeng, K. Lim, S. Pinel, M. M. Tentzeris, J. Laskar, "Design of compact stacked-patch antennas in LTCC multilayer packaging modules for wireless applications," IEEE Transactions on Advanced Packaging, Volume: 27, Issue: 4 , Nov. 2004, pp. 581-589.

# REFERENCES


1. C. Balanis, Antenna Theory: Analysis and Design, New York, John Wiley & Sons, Inc., 1997.

2. W. Stutzman, G. Thiele, Antenna Theory and Design, New York, John Wiley & Sons, Inc., 1998.

3. D. Pozar, D. Schubert, Microstrip Antennas: The Analysis and Design of Microstrip Antennas and Arrays, New Jersey, IEEE Press, 1995.

4. R. Garg, P. Bhartia, I. Bahl, A. Ittipiboon, Microstrip Antenna Design Handbook, Massachusetts, Artech House, Inc., 2002.

5. K. Lim, S. Pinel, M. Davis, A Sutono, C. Lee, D. Heo, A. Obatoynbo, J. Laskar, M. Tentzeris, R. Tummala, "RF-system-on-package (SOP) for wireless communications," IEEE Microwave Magazine, Volume: 3, Issue: 1, March 2002, pp. 88-99.

6. R. Tummala, Fundamentals of Microsystems Packaging, New York, The McGraw-Hill Companies, Inc., 2001

7. D. Pozar, "Microstrip antennas," Proceedings of the IEEE, Volume: 80, Issue: 1, Jan. 1992, pp. 79-91.

8. S. Consolazio, K. Nguyen, D. Biscan, K. Vu, A. Ferek, A. Ramos, "Low temperature cofired ceramic (LTCC) for wireless applications," IEEE MTT-S Symposium on Technologies for Wireless Applications, Feb. 1999, pp. 201-205.

9. L. Devlin, G. Pearson, B. Hunt, "Low-cost RF and microwave components in LTCC," Proceedings of MicroTech 2001, Jan. 2001, pp. 59-64.

10. D. Thompson, M. Tentzeris, J. Papapolymerou, S. Verdeyme, "Characterization of liquid crystal polymer (LCP) material and transmission lines on LCP substrates from 30-110 GHz," Transactions on Microwave Theory and Techniques, Nov. 2003.

11. K. Wong, Compact and Broadband Microstrip Antennas, New York, John Wiley & Sons, Inc., 2002.

12. I. Bahl, P. Bhartia, Microstrip Antennas, Massachusetts, Artech House, Inc., 1980.

13. S. Bokhari, J. Zurcher, J. Mosig, F. Gardiol, "A small microstrip patch antenna with a convenient tuning option," IEEE Transactions on Antennas and Propagation, Volume: 44, Issue: 11, Nov. 1996, pp. 1521-1528.

14. S. Dey, R. Mittra, T. Kobayashi, M. Itoh, S. Maeda, “Circular polarized meander patch antenna array,” IEEE Antennas and Propagation Society International Symposium, Volume: 2, July 1996, pp. 1100-1103.

15. K. Wong, J. Kuo, T. Chiou, “Compact microstrip antennas with slots loaded in the ground plane,” IEEE Antennas and Propagation Society International Symposium, Volume: 2, July 2001, pp. 732-735.

16. H. Wang, M. Lancaster, “Aperture-coupled thin-film superconducting meander antennas,” IEEE Transactions on Antennas and Propagation, Volume: 47, Issue: 5, May 1999, pp. 829-836.

17. M. Vaughan, K. Hur, R. Compton, “Improvement of microstrip patch antenna radiation patterns,” IEEE Transactions on Antennas and Propagation, Volume: 42, Issue: 6, June 1994, pp. 882-885.

18. R. Mittra, S. Dey, “Challenges in PCS design,” IEEE International Symposium 1999, Antennas and Propagation Society, Volume: 1, July 1999, pp. 544-547.

19. http://www.fcc.gov/cgb/sar/.

20. R. Waterhouse, S. Targonski, D. Kokotoff, “Design and performance of small printed antennas,” IEEE Transactions on Antennas and Propagation, Volume: 46, Issue: 11, Nov. 1998, pp. 1629-1633.

21. S. Targonski, R. B. Waterhouse, “An aperture coupled stacked patch antenna with 50% bandwidth,” IEEE Antennas and Propagation Society International Symposium, Volume: 1, July 1996, pp. 18-21.

22. P. Bhartia, I. Bahl, “A frequency agile microstrip antenna,” IEEE Antennas and Propagation Society International Symposium, Volume: 20, May 1982, pp. 304-307.

23. R. Waterhouse, N. Shuley, “Full characterisation of varactor-loaded, probe-fed, rectangular, microstrip patch antennas,” IEEE Proceedings on Microwaves, Antennas and Propagation, Volume: 141, Issue: 5, Oct. 1994, pp. 367-373.

24. M. du Plessis, J. Cloete, “Tuning stubs for microstrip-patch antennas,” IEEE Antennas and Propagation Magazine, Volume: 36, Issue: 6, Dec. 1994

25. C. Huang, J. Wu, K. Wong, “Cross-slot-coupled microstrip antenna and dielectric resonator antenna for circular polarization,” IEEE Transactions on Antennas and Propagation, Volume: 47, Issue: 4, April 1999, pp. 605-609.

26. H. Iwasaki, "A circularly polarized small-size microstrip antenna with a cross slot," IEEE Transactions on Antennas and Propagation, Volume: 44, Issue: 10, Oct. 1996, pp. 1399-1401.

27. P. Sharma, K. Gupta, "Optimized design of single feed circular polarized microstrip patch antennas," IEEE Antennas and Propagation Society International Symposium, Volume: 19, June 1981, pp. 19-22.

28. K. Carver, J. Mink, "Microstrip antenna technology," IEEE Transactions on Antennas and Propagation, Volume: 29, Issue: 1, Jan. 1981, pp. 2-24.

29. W. Richards, "Microstrip antennas," Chapter 10 in Antenna Handbook: Theory, Applications and Design, New York, Van Nostrand Reinhold Co., 1988.

30. Y. Hwang, Y. Zhang, G. Zheng, T. Lo, "Planar inverted F antenna loaded with high permittivity material," Electronic Letters, Volume: 31, Issue: 20, Sept. 1995, pp. 1710-1712.

31. C. Huang, J. Wu, K. Wong, "High-gain compact circularly polarised microstrip antenna," Electronic Letters, Volume: 34, Issue: 8, April 1998, pp. 712-713.

32. T. Kojiya, Y. Kuwahara, "Improvement of gain of the phased array antenna by the parasitic elements," IEEE Antennas and Propagation Society International Symposium, Volume: 3, July 2001, pp. 812-815.

33. M. El Yazidi, M. Himdi, J. Daniel, "Aperture coupled microstrip antenna for dual frequency operation," Electronic Letters, Volume: 29 Issue: 17, Aug. 1993, pp. 1506-1508.

34. K. Wong, Y. Lin, "Small broadband rectangular microstrip antenna with chip-resistor loading," Electronic Letters, Volume: 33, Issue: 19, Sept. 1997, pp. 1593-1594.

35. E. Levine, G. Malamud, S. Shtrikman, D. Treves, "A study of microstrip array antennas with the feed network," IEEE Antennas and Propagation, Volume: 37, no.4, April 1989, pp. 426-434.

36. J. James, P. Hall, Handbook of Microstrip Antennas, Vols. 1 and 2, London, UK, Peter Peregrinus, 1989.

37. S. Gao, L. W. Li, M. S. Leong, T. S. Yeo, "A broad-band dual-polarized microstrip patch antenna with aperture coupling," IEEE Transactions on Antennas and Propagation, Volume: 51, Issue: 4, April 2003, pp. 898-900.

38. L. Zaid, G. Kossiavas, J.-Y. Dauvignac, J. Cazajous, A. Papiernik, “Dual- Frequency and broad-band antennas with stacked quarter wavelength elements,” IEEE Transactions on Antennas and Propagation, Volume: 47, Issue: 4, April 1999, pp. 654-660.

39. R. L. Li, G. DeJean, M. M. Tentzeris, J. Laskar, “Development and analysis of a folded shorted-patch antenna with reduced size,” IEEE Transactions on Antennas and Propagation, Volume: 52, Issue: 4, Feb. 2004, pp. 555-562.